SYK and SYK-like models

Yuki Rea Hamano
4190858

Supervised by: Prof. Stefan Vandoren
Prof. Henk Stoof

Thesis submitted in partial fulfillment
of the requirements for the Degree of
Master of Science

Institute for Theoretical Physics
Utrecht University

June 2019

Abstract

The SYK model of Sachdev, Ye and Kitaev is a recent model of N Majorana fermions coupled via quartic random interaction. It has the extraordinary properties of being exactly solvable at large N, having emergent conformal symmetry in the IR, and exhibiting maximal quantum chaos. The confluence of these properties make SYK a highly attractive candidate for a solvable AdS/CFT correspondence. What's more, it was found to capture elements of non-Fermi-liquid behavior in strange metals. This thesis introduces the SYK model and discusses a recent variant, the SYK* model of Marcus and Vandoren. In the latter, the effective action is derived and branches of conformal solutions are discussed. The parameter space of SYK* is investigated for large and small $\frac{M}{N}$. The former reveals a phase separation and a critical point in the $T - \frac{M}{N}$ plane is claimed to exist.

La nature est une sphère infinie dont le centre est partout et la circonférence nulle part.

Nature is an infinite sphere whose center is everywhere and circumference nowhere.

Blaise PASCAL, *Pensées*

Acknowledgments

I would like to first and foremost thank my supervisors, Stefan and Henk. Their guidance throughout the length of this project has been invaluable. I so appreciate their patience and consideration in helping me with difficulties big and small. I am enormously grateful to have had the opportunity to work with and learn from the best.

Thank you to my parents, Yumiko and Michael. I have met many trials and hurdles in the course of this Master's. I could not have overcome half of them if not for your unwavering love and support. I love you both very much, and dedicate this thesis to you.

Finally, thank you to my friends, Little Athenians, Margherita, and Alejandro. It has been an unforgettable stay in Utrecht thanks to you guys. In our own unique ways, we have all come from far. Sharing this experience with you has been a great pleasure.

Contents

Chapter 1

Introduction

Strongly coupled many-body systems are notorious in theoretical physics for their unsolvability. These are systems in which the inter-species interactions are strong enough that the standard perturbation theory approach is rendered ineffective. Such systems are prominent in many areas from high-T_c superconductors in condensed matter to gauge theories in high-energy physics. While strongly coupled systems remain for the large part synonymous with intractability, sometimes the problem can be sidestepped.

This is the case of random spin systems, an agglomeration of quantum spins with all-to-all randomized interactions. Physical realizations of such systems are known as spin glassy phases of matter. Unlike crystalline-based spin models, glassy phases consist of structurally disordered frustrated magnets. The unique property of random quantum spin systems is that they are able to correlate nearby spins weakly just as far-off ones strongly. As a result, spin glasses have been extensively studied in the hope of elucidating the nature of their phase transitions.

This is specifically what Sachdev and Ye attempted to do in 1992 with the **SY model** [1]. It is a model of randomly coupled quantum Heisenberg magnets with infinite-range interaction described by

$$H = \frac{1}{\sqrt{M}} \sum_{i,\, j=1}^{N} J_{ij} \boldsymbol{S}_i \cdot \boldsymbol{S}_j, \tag{1.1}$$

where N is the number of sites, the couplings J_{ij} are independent Gaussian random variables, and the spins are in some representation of $SU(M)$. Previously it was shown that for $M = 2$ the model exhibited a zero-temperature spin-glass-order phase [2]. By promoting the spins to arbitrary representation $SU(M)$, Sachdev and Ye were able to acquire analytic control in the strong coupling and dual limits N, $M \gg 1$. In these limits, while keeping $\frac{N}{M} = \kappa$ fixed, they could interpolate between deep within the magnetically ordered spin-glass phase to well inside the spin-fluid phase. Some years later, Sachdev showed that a close parallel

exists between holographic metals near Reissner-Nordström black holes and the fractionalized Fermi-liquid phase of the lattice Anderson model, of which the SY model is a specific case [3]. The correlation functions in SY were found by representing the spin operators in terms of (Abrikosov) fermions,

$$S_i^{\alpha\beta} = (\psi^{\alpha\dagger}\psi^{\beta})_i$$

where ψ is a fermionic annihilation operators and $\alpha, \beta = 1, \ldots, M$ are group indices [1, 4]. Under such a mapping the SY Hamiltonian becomes one of four-fermion interactions.

This led Kitaev to propose - in a series of lectures given as recently as 2015 - a simpler yet nonetheless highly appealing variant of the SY model: the Sachdev-Ye-Kitaev or **SYK model** [5, 6]. It is a $0 + 1$ dimensional quantum mechanical model of N fermions with all-to-all quartic Gaussian-randomized self-interaction. The SYK Hamiltonian simplifies the four-fermion interactions in SY by using Majorana fermions:

$$H = -\frac{1}{4!}\sum_{i,j,k,l=1}^{N} J_{ijkl}\psi_i\psi_j\psi_k\psi_l. \tag{1.2}$$

There are several immediate reasons for studying the SYK model over the SY model. Replacing pairwise coupled spins by quartic interactions lessens the disorder effects per interaction; it is simpler than the SY model in that only a single large N limit is required rather than a dual limit. In spite of its apparent simplicity, the SYK model has garnered widespread research interest because it has been shown to possess three remarkable properties:

1. *Solvable at large N*: In the limit of large N all Feynman diagrams of order $O(1/N)$ and higher vanish. The set of surviving diagrams acquire an exceptionally simple form, known as "melon" diagrams. As a result of this major simplification, the n-point correlation functions can be calculated hence the theory is solvable.

2. *Conformal symmetry*: The SYK model enjoys emergent conformal symmetry in the infrared or strong coupling limit. This enables the use of powerful tools in conformal field theory such as the highly constrained form of the two- and higher- point correlators.

3. *Maximal chaos*: The degree of stability/instability in finite-temperature dynamical systems is quantified by the Lyapunov exponent λ. SYK saturates the instability bound of this exponent ($\lambda \leq 2\pi/\beta \equiv 2\pi k_{\mathrm{B}}T$) for large N theories. What is intriguing is the symbiosis of solvability and maximal chaos in the SYK model, a normally mutually exclusive pair of properties for classical systems [7].

Both SY and SYK belong to a class of models called **large-N models**. The purpose of such models is to simplify the pertubation theory expansion by using $1/N$ as the expansion parameter. This idea was initiated by 't Hooft who used a $1/N$-expansion in the context of quantum chromodynamics (QCD), the non-Abelian gauge theory underlying the strong interactions between quarks and gluons [8]. QCD displays asymptotic freedom, which is to say that as the energy scale increases the strength of a coupling constant g becomes asymptotically weaker. Conversely as energy scales decrease g becomes strong, thereby confining quarks and gluons into hadronic states. This is the reason why a standard perturbative expansion in the coupling constant g is disallowed for low energy scales in QCD. This limitation is partially overcome by augmenting the QCD gauge group from $SU(3)$ to $SU(N)$. When N is taken to be large, the resultant Feynman diagrams from the $1/N$ expansion acquired a greatly simplified topology: planar diagrams.

From a condensed-matter perspective, the SYK model has been shown to describe **non-Fermi-liquid** states of matter [9, 10]. Transport properties of many materials are well described by the celebrated Fermi-liquid theory (FLT), in which the quasi-particle idea plays an essential role. Yet the advent of progress in solid-state experiments has given rise to many exotic states of matter ill-described by FLT: cuprates, pnictides and heavy-fermion materials are some examples [11]. Their quasi-particles excitations are extremely short-lived, so much so that these "strange metals" are often said not to have quasi-particle description at all. The standard FLT toolkit can therefore not be used to understand non-Fermi liquids [12].

The fact that the SYK model exhibits maximal chaos suggests the presence of an underlying holographic dual. By the second item, it is believed to be a black hole in $1+1$ dilaton (or Jackiw-Teitelboim) gravity [4]. Such a duality is an example of what is more broadly coined an Anti-de Sitter/Conformal Field Theory correspondence or **AdS/CFT correspondence**. It conjectures the equivalence of a quantum field theory in flat spacetime to a string theory, the canonical example being the AdS_5/CFT_4 correspondence: $N = 4$ super Yang-Mills theory in $3+1$-dimensions is dynamically equivalent to type IIB superstring theory on $AdS_5 \times S^5$ [13]. Considered by many as being one of the most exciting discoveries in modern theoretical physics, the AdS/CFT correspondence has important implications in condensed matter as well: in some limit it becomes a strong-weak coupling duality. This means that an otherwise intractable strongly coupled many-body theory may be dual to a possibly amenable classical gravity theory [14].

There is one issue with interpreting the SYK model as being dual to black holes: it is a model with quenched random disorder. This means that to compute n-point correlators it is necessary to calculate the average over this disorder. This is done by way of replicating the system under consideration so as to be able to average those replicas. However, since real quantum systems do not have random interactions that are later disorder averaged over a probability distribution [7], it is

unlikely that the SYK model can provide answers to subtle questions about black holes [15]. Motivated by this reason, Witten proposed an SYK-like model without quenched disorder. This model, referred to as the Gurau-Witten model, is one of rank-3 tensor fields with $O(N)^3$ symmetry group [15, 16]. It is SYK-like in the sense that in the large N limit its two-point function is also dominated by melonic diagrams. Furthermore, it exhibits the same thermodynamic behavior as the SYK model. The hope is that such **tensor models** may provide insight on interpreting their holographic dual sector [17].[1]

Besides the Gurau-Witten tensor model, many **generalizations** of the SYK model have seen the light of day since Kitaev's famous talks. The most natural is the extension from quartic to q-fold interactions with $q \in \mathbb{Z}$. Because it lends itself well to other generalizations, many authors have adopted this extension *ab initio* [18]. Indeed, we will ourselves assume this extension throughout the majority of this thesis. Perhaps the most studied SYK-like model is the supersymmetric SYK or SUSY SYK model [19,20]. Numerous other generalizations exist: for example, extensions to higher dimensional SYK in field theory [21] or in lattice models [22,23]; a version with additional quadratic fermion hopping [24]; extensions that include multiple flavors of fermions, pure scalars, or complex fermions [9, 18].

One very recent generalization will be central to this thesis; the **SYK* model**[2] proposed by Marcus and Vandoren in 2018 [25]. In this version, to the existing N real Majorana fermions are added M auxiliary bosonic degrees of freedom with Yukawa-type interaction:

$$H = \frac{1}{2}\phi^a\phi^a - \frac{i}{2!}\sum_{a=1}^{M}\sum_{i,j=1}^{N} C_{ij}^a \phi^a \psi_i \psi_j. \tag{1.3}$$

The couplings C_{ij}^a, which define the dimensionful quantity J, are disorder averaged over a Gaussian distribution. The SYK* model too preserves the above-listed properties of SYK: solubility at large N and M, emergent conformal symmetry in the IR, and maximal saturation of chaotic behavior. Moreover the presence of the new free parameter M in the theory naturally paves the way for a study of the (potentially) rich parameter space. This was done in part by the original authors who found two branches of solutions for $M, N \gg 1$ but $\frac{M}{N}$ fixed at strong coupling $J \to \infty$. For $\frac{M}{N} \to \infty$ they found that the two branches converged to a unique conformal solution. However, it is also interesting to ask what the solutions to the Green's functions are in the regimes $\frac{M}{N} \gg 1$ and $\frac{M}{N} \ll 1$ when J is kept fixed (at finite coupling).

[1] Curiously, considering the SYK couplings J_{ijkl} as being a slowly-varying dynamical field from the start will produce the same diagrammatic structure [4], though as of yet this has not been found to be a fruitful route.

[2] This is not the officially recognized name of this SYK-like model. It is a name attributed by the author of this thesis.

This thesis will answer this question. As a whole, the thesis outline is as follows: In chapter 2 we give a detailed introduction to the SYK model. We derive the bare two-point function from the path-integral formalism. We then switch on the interactions and describe the resulting perturbative Feynman diagrams in subsection 2.2.2. We use the fact that the SYK model is a melonic theory to write down the self-energy. In the infrared limit the fermionic Green's function is solvable by virtue of conformal symmetry: we show this in subsection 2.2.4 and use it to find the finite-temperature Green's function in subsection 2.2.5. We discuss the $q = 2$ and $q \to \infty$ cases before briefly mentioning higher-point correlators (subsection 2.2.6 and section 2.3 respectively).

In chapter 3 we dive into the SYK* model of Marcus and Vandoren. In section 3.1, we describe its relation to the SYK model and the SUSY SYK model. Interestingly, SYK* also shows an affinity to a seemingly unrelated model of semi-holographic fermions. We will establish this later by comparing spectral functions in section 3.3. In section 3.2 we derive the exact expressions for the fermionic and bosonic self-energies by the saddle-point method. The conformal ansatz in the IR is used to find the two branches of conformal solutions, the "rational" and the "irrational" in subsection 3.2.4. In this section, we also discuss the spectral functions in SYK*. The saddle points will serve us in chapter 4 to explore the parameter space of SYK*. We present solutions to the Green's functions in the regimes where $\frac{M}{N} \gg 1$ and $\frac{M}{N} \ll 1$. The thesis concludes with a discussion and an outlook on future research.

Chapter 2

SYK model

In this chapter we review the SYK model and present several of its characteristic features. We illustrate the dominance of melon diagrams in SYK and show how the conformal symmetry arises in the infrared limit. We will not enter into the unwieldy details of the holographic dual description, for which there are already many references like the overview in [26]. Originally, the SYK model was incarnated as a theory of quartic interactions. In this chapter, however, we will use the now-common extension to q-point interactions (except for when it is more instructive to consider the case $q = 4$). There are two cogent reasons for doing this: (i) qualitatively, the model has the same distinctive properties for arbitrary q, and (ii) it allows for the study of special cases.

2.1 Introduction to the SYK model

The SYK Hamiltonian with q-fold interaction is given by

$$H = \frac{i^{q/2}}{q!} \sum_{i_1,\dots i_q=1}^{N} J_{i_1\dots i_q} \psi_{i_1} \cdots \psi_{i_q}, \tag{2.1}$$

where the Majorana fermions obey the usual anti-commutation relation $\{\psi_i, \psi_j\} = \delta_{ij}$ and the couplings $J_{i_1\dots i_q}$ are totally anti-symmetric upon interchange of two indices (i.e. $J_{i_1\dots i_m i_n \dots i_q} = -J_{i_1\dots i_n i_m \dots i_q}$ for $1 \leq n, m \leq q$). The factor of $i^{q/2}$ is required in order to preserve the Hermiticity of the Hamiltonian. For the same reason, q is restricted to the even integers. The factor of $1/q!$ accounts for all the ways of ordering the q operators in the summand. The sum over the indices is written explicitly; this is usually implied for repeated indices so we henceforth omit them. The couplings are seen as independent random variables drawn from a Gaussian distribution with mean and variance given by

$$\langle J_{i_1\dots i_q} \rangle = 0 \quad \text{and} \quad \langle J_{i_1\dots i_q} J_{j_1\dots j_q} \rangle = \frac{(q-1)!J^2}{N^{q-1}} \delta_{i_1 j_1} \cdots \delta_{i_q j_q}. \tag{2.2}$$

The factorial in the variance is chosen for later convenience while the scaling of N is chosen to obtain a non-trivial $N \gg 1$ limit. As noted by [27], the choice of this ensemble is not altogether arbitrary. While it is possible to retrieve the large N diagrammatic structure using any probability density (e.g. the simple Bernoulli distribution), non-Gaussian densities are not useful in finding the non-perturbative effective action by saddle point approach (see section 3.2). The SYK action follows as

$$S = \int d\tau \left(\frac{1}{2}\psi_i \dot{\psi}_i - \frac{i^{q/2}}{q!} J_{i_1 \ldots i_q} \psi_{i_1} \cdots \psi_{i_q} \right) \equiv S_0 + S_1, \tag{2.3}$$

where we are using the notation $\dot{\psi}_i = \partial \psi_i / \partial \tau$ and have defined the non-interacting and interacting parts of the action S_0 and S_1 respectively. By dimensional analysis we see that the canonical scale dimensions are $[\psi_i] = 0$ while $[J_{i_1 \ldots i_q}] = [J] = 1$. As we will shortly see in subsection 2.2.3, the fermions will flow towards an IR fixed point with dimension $\Delta = 1/q$.

2.2 Two-point function

In this section we solve for the two-point function or Green's function in the SYK model. The procedure followed is identical to that standard in the functional integral formulation of quantum field theory applied to $0 + 1$ dimensions.

2.2.1 Free theory

We first consider the non-interacting SYK model, i.e., only S_0 in eq. (2.3). After supplementing the SYK action with a Grassmannian source term, the path integral in the free theory is

$$Z_0[J] = \int \mathrm{D}[\psi] e^{-S_0 - \int d\tau J_i \psi_i} \tag{2.4}$$

$$= \int \mathrm{D}[\psi] \exp \left[- \int d\tau \left(\frac{1}{2}\psi_i \dot{\psi}_i + J_i \psi_i \right) \right], \tag{2.5}$$

where for the measure we are using the shorthand notation

$$\mathrm{D}[\psi] = \mathrm{D}[\psi_i] \, \mathrm{D}[\psi_2] \cdots \mathrm{D}[\psi_q]. \tag{2.6}$$

Expanding the real anti-commuting fields in terms of fermionic (odd) Matsubara frequencies $\omega_n = n\pi/\beta$ where $n \in 2\mathbb{Z} + 1$,

$$\psi_i(\tau) = \frac{1}{\beta} \sum_{n \in 2\mathbb{Z}+1} e^{-i\omega_n \tau} \psi_{i,n}, \tag{2.7}$$

the path integral becomes

$$Z_0[J] = \int \mathrm{D}[\psi] \exp\left[-\frac{1}{\beta} \sum_{n\in 2\mathbb{Z}+1} \left(\frac{1}{2}\psi_{i,n} i\omega_n \psi_{i,-n} + J_{i,n}\psi_{i,-n} \right) \right], \tag{2.8}$$

where we used that $\omega_{-n} = -\omega_n$. Next, by shifting the fields as $\psi_{i,n} \to \psi_{i,n} - J_{i,n}/(i\omega_n)$ we can easily complete the square:

$$Z_0[J] = \int \mathrm{D}[\psi] \exp\left(-\frac{1}{\beta} \sum_{n\in 2\mathbb{Z}+1} \frac{1}{2}\psi_{i,n}(i\omega_n)\psi_{i,-n} \right) \exp\left[\frac{1}{\beta} \sum_{n\in 2\mathbb{Z}+1} \frac{1}{2} J_{i,n} \left(\frac{1}{-i\omega_n} \right) J_{i,-n} \right]. \tag{2.9}$$

The path integral over the fermions is Gaussian so it can be readily evaluated. The proportionality constant coming from doing this is absorbed into the measure, as usual. The result is then

$$Z_0[J] = \exp\left[\frac{1}{\beta} \sum_{n\in 2\mathbb{Z}+1} \frac{1}{2} J_{i,n} \left(\frac{1}{-i\omega_n} \right) J_{i,-n} \right] \tag{2.10}$$

$$\equiv \exp\left(\frac{1}{2} \int \mathrm{d}\tau\, \mathrm{d}\tau' J_i(\tau) \Delta(\tau - \tau') J_i(\tau') \right) \tag{2.11}$$

where we defined the Euclidean time propagator as

$$\Delta(\tau - \tau') = \frac{1}{\beta} \sum_{n\in 2\mathbb{Z}+1} \frac{e^{-i\omega_n(\tau-\tau')}}{-i\omega_n} \tag{2.12}$$

The Green's function is defined as the expectation value of the time-ordered product of creation and annihilation operators:

$$\begin{aligned} G(\tau,\tau') &\equiv \langle \mathrm{T}[\psi_i(\tau)\psi_i(\tau')] \rangle \\ &= \theta(\tau-\tau')\langle \psi_i(\tau)\psi_i(\tau') \rangle - \theta(\tau'-\tau)\langle \psi_i(\tau')\psi_i(\tau) \rangle \end{aligned} \tag{2.13}$$

where $\mathrm{T}[\cdots]$ represents the time-ordering operator and $\langle\cdot\rangle$ denotes the thermal average. The Heaviside step function $\theta(x)$ is 1 for $x \geq 0$ and 0 for $x < 0$. The non-interacting Green's function is then given by

$$\begin{aligned} G_0(\tau,\tau') &= \frac{1}{Z_0[0]} \frac{\delta}{\delta J_i(\tau')} \frac{\delta}{\delta J_i(\tau)} Z_0[J] \bigg|_{J=0} \\ &= \Delta(\tau - \tau'). \end{aligned} \tag{2.14}$$

Therefore, in frequency space and in Euclidean time (at $T = 0$) we have

$$G_0(i\omega_n) = \frac{1}{-i\omega_n} \quad \text{and} \quad G_0(\tau - \tau') = \frac{1}{2}\,\mathrm{sgn}(\tau - \tau'), \tag{2.15}$$

where $\mathrm{sgn}(x)$ is the sign-function: it equals 1 for $x > 0$, 0 for $x = 0$, and -1 for $x < 0$. The bare fermionic Green's functions in eq. (2.15) are seen to be odd in frequency and imaginary time as required by their statistics.

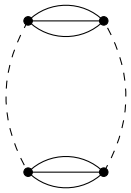

Figure 2.1: Leading order correction to inter-replica interactions. The top and bottom parts of the diagram have different replica indices. One can show that this goes as $\sim \frac{1}{N}$.

2.2.2 Interacting theory

We now turn on the interaction and consider the full SYK model, i.e., both S_0 and S_I in eq. (2.3). As was alluded to in the introduction, in order to compute the two-point function (or n-point function for that matter) it is necessary to perform the disorder average over these correlators. This involves computing $\langle \log Z \rangle_{\mathrm{D}}$ (where the chevron braces $\langle \cdot \rangle_{\mathrm{D}}$ represent the disorder average). The problem that arises is that in general $\langle \log Z \rangle_{\mathrm{D}} \neq \log \langle Z \rangle_{\mathrm{D}}$. To deal with this we use a common trick called the "replica trick". It is based on the simple formula,

$$\langle \log Z \rangle_{\mathrm{D}} = \lim_{n \to 0} \frac{1}{n} \log \langle Z^n \rangle_{\mathrm{D}}. \tag{2.16}$$

This formula is handy because for integer n the right-hand side essentially replicates the system n times with exactly the same disorder realization (quenched disorder). This can easily be computed by integrating out the Gaussian-random disorder. However, in general, the process of integrating over the disorder will lead to couplings between different replicas [28]. But in SYK such couplings are actually subdominant for $N \gg 1$ so that inter-replica diagrams do not contribute (see fig. 2.1). This replica diagonal ansatz greatly facilitates the computation of n-point functions. In this thesis, we will assume this symmetry and thereby avoid writing out replica indices everywhere.

In this subsection, we privilege clarity over generality by setting $q = 4$: this makes the Feynman diagrams more legible. Of course the entirety of the reasoning below can be carried over to the case of arbitrary q. For $q = 4$ the Gaussian statistics reduce to

$$\langle J_{ijkl} \rangle = 0 \quad \text{and} \quad \langle J_{ijkl} J_{mnop} \rangle = \frac{3! J^2}{N^3} \delta_{im} \delta_{jn} \delta_{ko} \delta_{lp}. \tag{2.17}$$

Any diagram is created by joining propagators to vertices using the following Feynman rules:

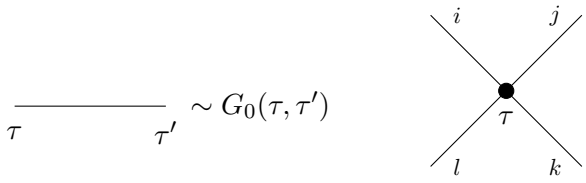

The question now is, what kind of Feynman diagrams contribute to the 1-particle irreducible (1PI) self-energy? In particular, how do they behave in the limit of $N \gg 1$? To answer this we will look at a few elementary diagrams and calculate their contributions. In the following we will avoid cluttering the expressions with propagators and τ-integrals. As a first example, let us consider a very simple diagram appearing in this theory shown in fig. 2.2. It is the simplest possible correction to the two-point function and is expressed as

$$\frac{(4)(3)}{4!} \sum_{j=1}^{N} \langle J_{ijji} \rangle_{\mathrm{D}} = 0, \tag{2.18}$$

where we denote the external lines with index i. Note the sum over the internal loop index $1 \leq j \leq N$ in analogy with field theory integrals over internal loop momenta. We write them explicitly. In this case, the result is zero because the Gaussian distribution is 0-centered. This illustrates the fact that all diagrams with an odd number of vertices vanish. That being said, let us consider 1PI diagrams with two vertices; there are only two and they are shown in fig. 2.3. The expression for the diagram in fig. 2.3a is

$$\frac{4^2 3^2}{4!^2} \sum_{j,k,l} \langle J_{ijki} J_{ljkl} \rangle_{\mathrm{D}} = \frac{4^2 3^2}{4!^2} \frac{3! J^2}{N} = \frac{3}{2} \frac{J^2}{N}. \tag{2.19}$$

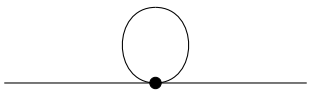

Figure 2.2: The simplest correction admissible by this model.

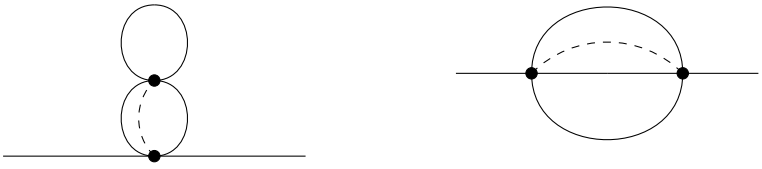

(a) (b)

Figure 2.3: The only two J^2 corrections to the self-energy. The dashed lines in the figures are used to indicate which pairs of vertices are being disorder averaged.

Although this diagram survives the disorder averaging, it will not survive the large N limit; it is a subdominant contribution. The diagram in fig. 2.3b is given by

$$\frac{4^2 3!}{4!^2} \sum_{j,\,k,\,l} \langle J_{ijkl} J_{ijkl} \rangle_{\mathrm{D}} = \frac{4^2 3!}{4!^2} 3! J^2 = J^2. \tag{2.20}$$

We see that the result is independent of N so that this will have a non-vanishing contribution to the self-energy. We next consider diagrams with four vertices; two (distinct) are shown in fig. 2.4. The diagrams in fig. 2.4b and fig. 2.4c are the same as in fig. 2.4a except the disorder average "contractions" are different. The diagram in fig. 2.4a is expressed as

$$\frac{4^4 3!^2}{4!^4} \sum_{j,\,\ldots,\,p} \langle J_{ijop} J_{inop} \rangle_{\mathrm{D}} \langle J_{jklm} J_{nklm} \rangle_{\mathrm{D}} = \frac{4^4 3!^2}{4!^4} 3!^2 J^4 = J^4 \tag{2.21}$$

We have found another nonzero contribution to the self energy at large N. One can show that the diagrams in fig. 2.4b and fig. 2.4c are proportional to $1/N^2$ and $1/N^5$ respectively. Finally, we compute the diagram in fig. 2.4d:

$$\frac{4^4 3!^2}{4!^4} \sum_{j,\,\ldots,\,p} \langle J_{ijkm} J_{ijlp} \rangle_{\mathrm{D}} \langle J_{klon} J_{mpon} \rangle_{\mathrm{D}} = \frac{4^4 3!^2}{4!^4} \frac{3!^2 J^2}{N^2} = \frac{J^2}{N^2}, \tag{2.22}$$

which is subdominant. From the above computations, observe that only a particular subset of diagrams survive the large N limit. This is not a coincidence; all the nonzero contributions to the two-point function in SYK belong to a class of diagrams known as melon diagrams (those in 2.3b and 2.4a are examples). Said differently, the 1PI self-energy consists solely of iterated melonic diagrams. This means substituting a propagator G_0 in a diagram by the combination $G_0 \Sigma G_0$. For example

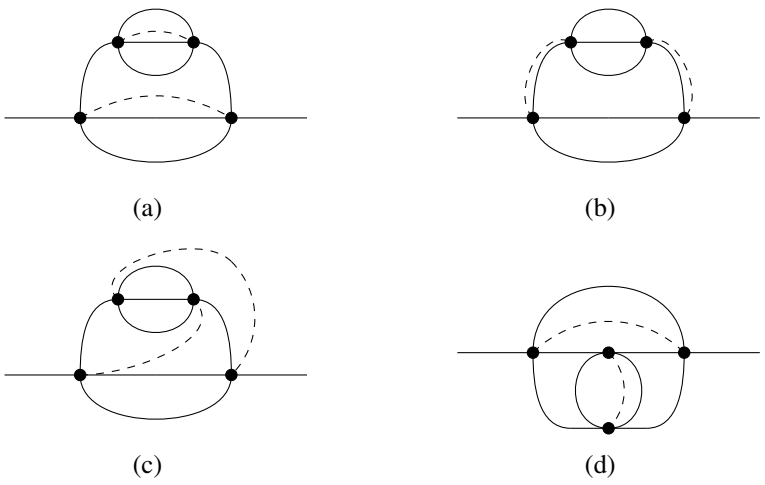

Figure 2.4: Some order J^4 corrections to the self energy.

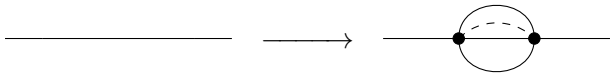

Figure 2.5: The iterative construction of melonic diagrams.

doing this with the upstairs propagator in fig. 2.3b yield the diagram in fig. 2.4a. This process of iteration is shown in fig. 2.5; it is a defining property of melonic diagrams. A diagram that cannot be reached by this process is necessarily non-melonic. This essentially describes the Schwinger-Dyson (SD) recursion relation

$$\begin{aligned} G(\tau,\tau') = G_0(\tau,\tau') + \int d\tilde{\tau} d\tilde{\tau}' G_0(\tau,\tilde{\tau}) \Sigma(\tilde{\tau},\tilde{\tau}') G(\tilde{\tau}',\tau') \\ \Sigma(\tau,\tau') = J^2 G(\tau,\tau')^3 \end{aligned} \tag{2.23}$$

as shown in fig. 2.6. The results can straightforwardly be generalized to q-fold interaction: [1]

$$\Sigma(\tau,\tau') = J^2 G(\tau,\tau')^{q-1}. \tag{2.24}$$

Melonic dominance is a characteristic feature of SYK and SYK-like models; the self-energy is always of a considerably simple form, as in eq. (2.24). In the next section, we exploit this trait and find a solution to eq. (2.23) by going to the infrared limit. For a schematic introduction to the subject of Feynman diagrams in the SYK model, the reader is directed to [7]. There, the vertex legs are labelled not by indices but by colors and in the language of colored tensor models, Feynman diagrams become 4-colored graphs. Lastly, for a rigorous proof using graph theory of the large-N melonic dominance in SYK the reader is referred to [29].

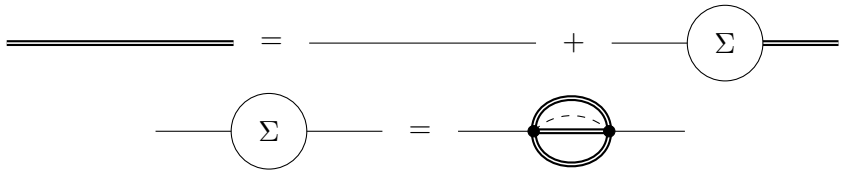

Figure 2.6: A graphical representation of the Schwinger-Dyson equation in the SYK model for $q = 4$. The double and single lines denote the interacting and bare Green's function respectively.

[1] The origin of the fruity nomenclature should now be clear. The $q-1$ propagators joining two vertices can be likened to the lines joining the North and South of a melon's surface.

2.2.3 Infrared limit

In the infrared (IR), or equivalently, the strong-coupling or low-energy limit ($N \gg \beta J \gg 1$ and $J \gg \omega_n$) the full Green's function can be exactly solved. As a result of eq. (2.24), the bare Green's function becomes negligible compared to the self-energy so that the SD equation in frequency space reduces to

$$\begin{aligned} G(i\omega_n) &= \frac{1}{G_0(i\omega_n)^{-1} - \Sigma(i\omega_n)} \\ &\approx \frac{-1}{\Sigma(i\omega_n)}. \end{aligned} \tag{2.25}$$

Inserting the self-energy we found into the Euclidean-time version of the above we get

$$-\delta(\tau - \tau') = J^2 \int d\tilde{\tau} G(\tau, \tilde{\tau}) G(\tilde{\tau}, \tau')^{q-1}. \tag{2.26}$$

We now use the fact that the Green's function has conformal symmetry (see subsection 2.2.4). Intuitively this follows from taking the IR limit, i.e., sending the only dimensionful quantity in the model to be very large. In conformal field theories, the high degree of symmetry completely constrain the form the two-point function can have. For a fermionic bilocal at $T = 0$, this form is given by the conformal ansatz:

$$G(\tau, \tau') = A \frac{\operatorname{sgn}(\tau - \tau')}{|\, \tau - \tau' \,|^{2\Delta}}, \tag{2.27}$$

where A and Δ (the conformal dimension) are constants to be determined. We do so promptly by inserting the ansatz into eq. (2.26). This yields

$$-\delta(\tau - \tau') = J^2 A^q \int d\tilde{\tau} \frac{\operatorname{sgn}(\tau - \tilde{\tau})}{|\, \tau - \tilde{\tau} \,|^{2\Delta}} \frac{\operatorname{sgn}(\tilde{\tau} - \tau')}{|\, \tilde{\tau} - \tau' \,|^{2\Delta(q-1)}} \tag{2.28}$$

where we used that $\operatorname{sgn}(\tau - \tau')^{q-1} = \operatorname{sgn}(\tau - \tau')$ since q is even. At zero-temperature we can use the Fourier transform,

$$\frac{\operatorname{sgn}(\tau - \tau')}{|\, \tau - \tau' \,|^{2\Delta}} = \int \frac{d\omega}{2\pi} e^{-i\omega(\tau - \tau')} i 2^{1-2\Delta} \sqrt{\pi} \frac{\Gamma(1-\Delta)}{\Gamma(\frac{1}{2} + \Delta)} |\, \omega \,|^{2\Delta - 1} \operatorname{sgn}(\omega), \tag{2.29}$$

to write eq. (2.28) in Fourier space:

$$-1 = -J^2 A^4 2^{2-2\Delta q} |\, \omega \,|^{2-2\Delta q} \frac{\Gamma(1-\Delta)}{\Gamma(\frac{1}{2} + \Delta)} \frac{\Gamma(1-(q-1)\Delta)}{\Gamma(\frac{1}{2} + (q-1)\Delta)}. \tag{2.30}$$

By power counting we find the conformal dimension $\Delta = 1/q$ and by using known properties of the Γ-function we can solve for the constant A. Thus, we obtain the exact conformal solution to the full Green's function

$$G_c(\tau, \tau') = \left(\frac{\frac{1}{2} - \frac{1}{q}}{J^2 \pi} \tan\left(\frac{\pi}{q}\right) \right)^{\frac{1}{q}} \frac{\operatorname{sgn}(\tau - \tau')}{|\, \tau - \tau' \,|^{2/q}}, \tag{2.31}$$

valid in the IR regime. This is one of the many solutions in the space of conformal solutions related to each other at no cost by reparametrizations.

2.2.4 Conformal symmetry

In the previous section we exploited the conformal invariance to obtain the IR solution to the Green's function eq. (2.31). We now justify this by showing that eq. (2.26) is indeed invariant under an arbitrary reparametrization

$$\tau \longrightarrow f(\tau) \quad \text{and} \quad \tau' \longrightarrow f(\tau'). \tag{2.32}$$

It suffices to show that under such a transformation the Green's function transforms as

$$G(\tau,\tau') \longrightarrow G(f(\tau),f(\tau')) = \left|\frac{df(\tau)}{d\tau}\right|^{-\Delta}\left|\frac{df(\tau')}{d\tau'}\right|^{-\Delta} G(\tau,\tau'). \tag{2.33}$$

We start by letting $G(\tau,\tau')$ be a solution to eq. (2.26). Then we perform the transformation prescribed in eq. (2.32):

$$-\delta(f(\tau)-f(\tau')) = J^2\int\left|\frac{df(\tilde{\tau})}{d\tilde{\tau}}\right| d\tilde{\tau} G(f(\tau),f(\tilde{\tau}))G(f(\tilde{\tau}),f(\tau'))^{q-1}. \tag{2.34}$$

By the identity

$$\delta(f(x)-f(x_0)) = \frac{1}{\left|\frac{df(x_0)}{dx}\right|}\delta(x-x_0) \tag{2.35}$$

we get

$$\begin{aligned}-\delta(\tau-\tau') = J^2\int d\tilde{\tau}&\left(\left|\frac{df(\tau)}{d\tau}\right|^{\frac{1}{q}}\left|\frac{df(\tilde{\tau})}{d\tilde{\tau}}\right|^{\frac{1}{q}} G(f(\tau),f(\tilde{\tau}))\right)\\ &\left(\left|\frac{df(\tilde{\tau})}{d\tilde{\tau}}\right|^{\frac{1}{q}}\left|\frac{df(\tau')}{d\tau\prime}\right|^{\frac{1}{q}} G(f(\tilde{\tau}),f(\tau'))^{q-1}\right)^{q-1},\end{aligned} \tag{2.36}$$

from which we see that eq. (2.26) is invariant provided the Green's functions transforms as in eq. (2.33).

Since we are in $0+1$ dimensions, this is the same as invariance under diffeomorphisms because $\text{Conf}_1(\mathbb{R}) \simeq \text{Diff}_1(\mathbb{R})$.

2.2.5 Thermal Green's function

The solution eq. (2.31) holds at zero temperature. Nonetheless, we can use the reparametrization invariance proved in the previous section to define a mapping from the imaginary strip to the thermal circle. This is achieved by the choice

$$\tau \longrightarrow f(\tau) = \tan\left(\frac{\pi\tau}{\beta}\right) \quad \text{and} \quad \tau' \longrightarrow f(\tau') = \tan\left(\frac{\pi\tau'}{\beta}\right). \tag{2.37}$$

The computation is straightforward. Letting $T = \pi\tau/\beta$ (likewise for T'),

$$\begin{aligned} &G_\beta(\tau,\tau') \\ &= \left|\frac{df(\tau)}{d\tau}\right|^\Delta \left|\frac{df(\tau')}{d\tau\prime}\right|^\Delta G_c(f(\tau),f(\tau')) \\ &= \left|\frac{\pi}{\beta}\frac{1}{\cos(T)^2}\right|^\Delta \left|\frac{\pi}{\beta}\frac{1}{\cos(T')^2}\right|^\Delta \left(\frac{\frac{1}{2}-\Delta}{J^2\pi}\tan(\pi\Delta)\right)^\Delta \frac{\operatorname{sgn}\big(\tan(T)-\tan(T')\big)}{\Big|\tan(T)-\tan(T')\Big|^{2\Delta}} \\ &= \left(\frac{\pi}{\beta}\sqrt{\frac{\frac{1}{2}-\Delta}{J^2\pi}\tan(\pi\Delta)}\right)^{2\Delta} \frac{\operatorname{sgn}(\tau-\tau')}{\left|\sin\left(\frac{\pi\tau}{\beta}-\frac{\pi\tau'}{\beta}\right)\right|^{2\Delta}}. \end{aligned} \tag{2.38}$$

where $\Delta = 1/q$, as before. Thus we have the nonzero temperature or thermal Green's function in SYK. This is an important quantity to know if one wishes to better understand the connection with the thermodynamics of extremal black holes.

The explicit result eq. (2.38) reintroduces an energy scale into the model, thereby spontaneously breaking the conformal symmetry. This means that the two-point function is not invariant under the whole conformal group $\mathrm{Conf}_1(\mathbb{R})$ but only under the smaller group $\mathrm{SL}_2(\mathbb{R})$. It is this spontaneous symmetry breaking that gives rise to low-temperature Nambu-Goldstone modes described by an effective Schwarzian action.

2.2.6 $q = 2$ and $q \to \infty$

In this brief interlude we present the special cases when $q = 2$ and $q \to \infty$, for which the two-point functions are analytically available. We begin with the former. For $q = 2$ the SYK model reduces to a free random-mass matrix model. The self energy becomes proportional to the Green's function itself:

$$\Sigma(\tau,\tau') = J^2 G(\tau,\tau'). \tag{2.39}$$

The Schwinger-Dyson equation turns into a quadratic equation in the Green's function, which is solved by

$$G(i\omega_n) = \frac{i\omega_n}{2J^2}\left(-1+\sqrt{1+\frac{4J^2}{\omega_n^2}}\right). \tag{2.40}$$

In terms of a diagrammatic expansion, this corresponds to the sum of all diagrams with non-crossing disorder-averaged dashed lines (see fig. 2.7) given by

$$G(i\omega) = G_0 \sum_{n=0}^{\infty} C_n \Big[JG_0(i\omega_n)\Big]^{2n}, \tag{2.41}$$

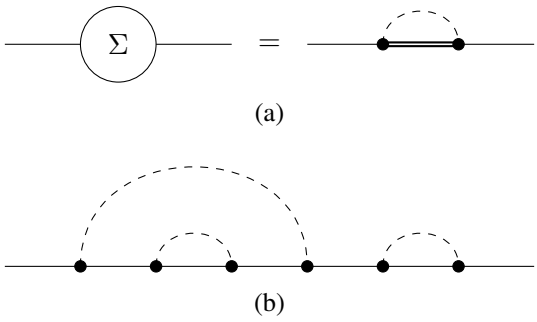

Figure 2.7: "Rainbow" diagrams in the $q = 2$ SYK model. Solid lines denote fermion, dashed lines denote disorder averaging. fig. 2.7a represents the 1PI self-energy in eq. (2.39) graphically while fig. 2.7b shows an order J^6 correction to the two-point function.

where C_n is the n^{th} Catalan number[2],

$$C_n = \frac{1}{n+1}\binom{2n}{n}. \tag{2.42}$$

As an aside, we remark that although the sum above over rainbow diagrams holds for $N \gg 1$, the random mass matrix model is also solvable for finite N. The limiting behavior in the latter coincides with eq. (2.40) [18].

The two-point function also simplifies drastically in the limit of $q \to \infty$. Expanding the IR Green's function eq. (2.31) to order $1/q$ we find

$$G(\tau, 0) = \frac{1}{2}\operatorname{sgn}(\tau)\Big(1 + \frac{1}{q}g(\tau) + \dots\Big), \tag{2.43}$$

where $g(\tau)$ is some function (independent of q) soon to be determined. Note that time-translation invariance was used to set $\tau' = 0$. Equally, we expand the self-energy eq. (2.24):

$$\Sigma(\tau, 0) = J^2\Big(\frac{1}{2}\Big)^{q-1}\operatorname{sgn}(\tau)e^{g(\tau)}(1 + \dots). \tag{2.44}$$

We now write eq. (2.43) in Matsubara frequency space as

$$\begin{aligned}\frac{1}{G(i\omega_n)} &= \frac{1}{\frac{1}{-i\omega_n} + \frac{1}{2q}h(i\omega_n)} \\ &= \frac{-i\omega_n^{\text{F}}}{1 - \frac{i\omega_n^{\text{F}}}{2q}h(i\omega_n^{\text{F}})} \\ &= -i\omega_n + \frac{(i\omega_n^{\text{F}})^2}{2q}h(i\omega_n^{\text{F}}),\end{aligned} \tag{2.45}$$

[2]Catalan numbers are prominent in combinatorial mathematics. One interpretation casts C_n as the number of ways n pairs of parentheses can be correctly ordered e.g. $C_3 = 5$: ()()(), ((())), (()()), ()(()), and (())(). In this sense, the disorder lines in fig. 2.7b are the parentheses.

where $h(i\omega_n)$ denotes the Matsubara expansion of the product $\mathrm{sgn}(\tau)g(\tau)$. By the SD equation this must be equal to $-i\omega_n - \Sigma(\tau)$. Comparing this with eq. (2.45) and using eq. (2.44) in frequency space we see that

$$\partial_\tau^2\Big(\mathrm{sgn}(\tau)g(\tau)\Big) = qJ^2\Big(\frac{1}{2}\Big)^q \mathrm{sgn}(\tau)e^{g(\tau)}, \tag{2.46}$$

where the basic property of Fourier transforms $\mathfrak{F}\{d^2f(\tau)/d\tau^2\} = (-i\omega_n)^2\mathfrak{F}\{f(\tau)\}$ was used. The solution to this differential equation determines the function $g(\tau)$. To make this equation well-defined in the limit of large q, we can scale J such that the combination $qJ^2\Big(\frac{1}{2}\Big)^q$ is kept fixed. We impose the boundary conditions $g(0) = g(\beta) = 0$ to ensure that at small time separations we recover free fermions. Then, the boundary value problem is solved by

$$e^{g(\tau)} = 2\ln\left(\frac{\cos\big(\frac{\pi\nu}{2}\big)}{\cos\Big(\frac{\pi\nu}{2} - \frac{|\tau|}{\beta}\Big)}\right) \tag{2.47}$$

where ν is determined from $\pi\nu/\cos\big(\frac{\pi\nu}{2}\big) = \sqrt{q/2^{q-1}}J\beta$.

2.3 Higher-point correlators

The unique diagrammatic stucture of the SYK model is not only limited to the two-point function. To leading order in $1/N$, the four-point correlation functions can be entirely described as a sum of so-called "ladder" diagrams. In this section, we sketch an outline of the treatment of four-point functions in the SYK model for $q = 4$ (based on [30]).

First we state that $(2n+1)$-point functions do not exist in the SYK model. This is because it is impossible to create a connected Feynman graph having $2n + 1$ external lines with only even vertices. So the SYK model only admits $2n$-point correlation functions. Notice that $2n$-point function can actually be thought of as the result of successively cutting internal propagators in melon diagrams.

Just as incoming and outgoing fields must have matching indices by disorder averaging, so too must four-point functions come with paired indices. The most general non-vanishing four-point function one can write down is

$$\langle \mathrm{T}[\psi_i(1)\psi_i(2)\psi_j(3)\psi_j(4)]\rangle \tag{2.48}$$

where we use the shorthand $1 = \tau_1$, $2 = \tau_2$, etc. It is then commonplace to average over these indices by

$$\frac{1}{N^2}\sum_{i,j=1}^{N}\langle \mathrm{T}[\psi_i(1)\psi_i(2)\psi_j(3)\psi_j(4)]\rangle = G(1,2)G(3,4) + \frac{1}{N}\mathcal{F}(1,2,3,4) + \mathcal{O}\Big(\frac{1}{N^2}\Big). \tag{2.49}$$

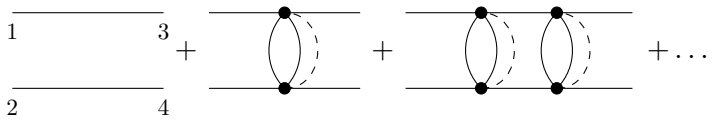

Figure 2.8: The first few ladder diagrams contributing the the four-point function at order $1/N$. Every line denotes the full propagator, dressed by melons as we have previously seen. The sum should also include minus the diagrams with $3 \leftrightarrow 4$.

On the right-hand side is a power series in $1/N$ where the first term are two disconnected propagators (essentially the free four-point function) while contained inside $\mathcal{F}(1,2,3,4)$ are all non-trivial leading order corrections. It can be shown that $\mathcal{F}(1,2,3,4)$ consist of a sum of ladder diagrams with arbitrary numbers of rungs (see fig. 2.8); all other kinds of diagrams are of sub-leading order. Denoting a ladder with n rungs as $\mathcal{F}_n(1,2,3,4)$, the sum over all ladders is obviously

$$\mathcal{F}(1,2,3,4) = \sum_{n=0}^{\infty} \mathcal{F}_n(1,2,3,4). \tag{2.50}$$

The usual strategy to perform this sum is to introduce the kernel

$$K(1,2,3,4) = -J^2(q-1)G(1,3)G(2,4)G(3,4)^{q-2}, \tag{2.51}$$

whose action is to generate rungs on ladders (as the self-energy adds melons to propagator) by

$$\mathcal{F}_{n+1}(1,2,3,4) = \int d\tau d\tau' K(1,2,\tau,\tau')\mathcal{F}_n(\tau,\tau',3,4), \tag{2.52}$$

as shown in fig. 2.9. Using this, eq. (2.50) can be written as

$$\mathcal{F} = \sum_{n=0}^{\infty} K^n \mathcal{F}_0 = \frac{1}{1-K}\mathcal{F}_0. \tag{2.53}$$

The above involved using the geometric series on the kernel operator. However as defined in eq. (2.51), the kernel is not symmetric under the exchange $(1,2) \leftrightarrow (3,4)$. One can remedy this by conjugating it between powers of Green's functions:

$$\tilde{K}(1,2,3,4) = |G(1,2)|^{\frac{q-2}{2}} K(1,2,3,4) |G(3,4)|^{\frac{2-q}{2}}. \tag{2.54}$$

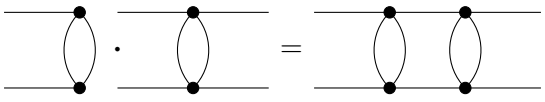

Figure 2.9: The kernel generates a rung on a ladder by integrating over the rung-endpoints.

Because the kernel is now symmetric, we are sure that there is a complete eigenbasis associated to $\tilde{K}$, which in turn facilitates the inversion. The next steps of the calculation are more involved and in general the full derivation of four-point correlation functions is rather lengthy. We will not delve into it here; instead we comment on other higher-point functions.

All higher $2n$-point correlation functions in the SYK model are made from gluing together lower $2n$-point functions. For example, the six-point function is composed of three four-point functions. In eight-point functions the six-point function plays the role of the interaction vertex such that the "tree level" diagram is essentially the eight-point function. In this sense all point correlation functions of the model are known; this is why the SYK model is often said to be exactly solvable [17, 30, 31].

Chapter 3

SYK* model

In this chapter we introduce a recent variant of the SYK model, the SYK* model, due to Marcus and Vandoren [25]. It is qualitatively similar to the original model in that it is dominated by melonic diagrams, enjoys near conformal symmetry in the IR, and exhibits maximal chaos. As we will see however there are also some important differences between the two models: (i) the SYK* model predicts two families of conformal solutions in the IR whereas a single explicit solution was found in the original SYK, and (ii) SYK* displays a phase transition in the $\frac{M}{N} \gg 1$ regime for fixed J. The second item is a novelty of the SYK* model; it results from introducing the tunable parameter M into the theory.

The SYK* model consists of a system of N Majorana fermions coupled to M auxiliary bosons through all-to-all Gaussian-random q-fold Yukawa-type interaction, described by the following Hamiltonian[1]

$$H = \frac{1}{2}\phi^a\phi^a - \frac{i}{(q-1)!}\sum_{a=1}^{M}\sum_{j_1=1}^{N}\cdots\sum_{j_{q-1}=1}^{N} C^a_{j_1\ldots j_{q-1}}\phi^a\psi_{j_1}\cdots\psi_{j_{q-1}}, \qquad (3.1)$$

where again the fermionic anti-commutation relations hold: $\{\psi_i, \psi_j\} = \delta_{ij}$ and the coupling is now anti-symmetric upon interchange of its lower indices ,i.e., $C^a_{i_1\ldots i_n i_m\ldots i_{q-1}} = -C^a_{i_1\ldots i_m i_n\ldots i_{q-1}}$ for $i_1 \leq n < m \leq i_{q-1}$. The factors i is related to safe-guarding the Hermiticity of the Hamiltonian and the $\frac{1}{(q-1)!}$ cancels the number of equivalent permutations of the fermions. Note that although we still speak of q-point interaction (between 1 boson and $q-1$ fermions), we should remember that q must be taken odd as opposed to SYK where q was taken even. Following the convention set by Marcus and Vandoren, the fermionic (bosonic) indices are denoted by i, j, etc. (a, b, etc.), and sum to N (M) as shown in eq. (3.1). We will refrain from writing these sums out from now on. The couplings $C^a_{i_1\ldots i_{q-1}}$ are once again drawn randomly from a Gaussian distribution with the following

[1]Marcus and Vandoren studied the case $q = 3$. Here we will mostly stick with arbitrary q, though for pedagogical reasons we sometimes revert back to $q = 3$.

mean and variance:

$$\begin{aligned}&\langle C^a_{i_1\ldots i_{q-1}}\rangle = 0,\\ &\langle C^a_{i_1\ldots i_{q-1}} C^b_{j_1\ldots j_{q-1}}\rangle = \frac{(q-1)!J}{N^{q-3/2}M^{1/2}}\delta^{ab}\delta_{i_1 j_1}\cdots\delta_{i_{q-1}j_{q-1}}.\end{aligned} \tag{3.2}$$

The discussion of the free theory is unchanged from the SYK model except that we now have a free boson propagator. It is easy to see that

$$G^0_\phi(i\omega^{\mathrm{B}}_n) = -1 \quad \text{and} \quad G^0_\phi(\tau,\tau') = -\delta(\tau-\tau'), \tag{3.3}$$

where $\omega^{\mathrm{B}}_n = (2n)\pi/\beta$ denote bosonic (even) Matsubara frequencies. The bosons are seen to be non-dynamical in SYK*. A Legendre transform yields the SYK* Lagrangian:

$$L = \frac{1}{2}\psi_i\dot{\psi}_i - \frac{1}{2}\phi^a\phi^a + \frac{i}{(q-1)!}C^a_{j_1\ldots j_{q-1}}\phi^a\psi_{j_1}\cdots\psi_{j_{q-1}}. \tag{3.4}$$

The SYK* model's diagrams are also dominated by melons. In fig. 3.1 are the first-order corrections to the 1PI bosonic and fermionic self-energies. Using the Feynman rules in this theory, one can easily show that fig. 3.1a is proportional to $\sqrt{\frac{N}{M}}$ and fig. 3.1b is proportional to $\sqrt{\frac{M}{N}}$. Thus for large N, M, and keeping $\frac{M}{N}$ fixed, these diagrams give nonzero contributions. In section 3.2, we will confirm this by deriving the exact self-energies using the saddle point method.

3.1 Relation to other models

When the number of fermions and bosons are the same ($N = M$), the SYK* model is related to the $\mathcal{N} = 1$ supersymmetric SYK model for N, $M \gg J\tau \gg 1$ [19]. The condition $N = M$ is necessary to have supersymmetry since fermions are bosons' superpartners and vice versa. That is, they transform into each other under

(a) (b)

Figure 3.1: The only J^2-order corrections to the bosonic and fermionic self energy for the case of $q = 3$ with one wiggly boson line and two solid fermion line. The dashed lines again denote which vertices are being disorder averaged with which.

supersymmetry transformations. Under this condition the $q = 3$ supersymmetric SYK model has Lagrangian

$$L = \sum_{i=1}^{N} \left(\frac{1}{2}\psi_i \dot{\psi}_i - \frac{1}{2}\phi^a \phi^a + \sum_{1 \leq i,j \leq N} C^a_{ij} \phi^a \psi_i \psi_j \right), \tag{3.5}$$

where the sums over indices run from 1 to $N(= M)$. A thorough introduction of the SUSY SYK model can be found in the authoritative study by Fu et al [19, 25].

The SYK* model can also simply be seen as a generalization of the SYK model. This is done by integrating out the bosonic degrees of freedom in SYK* as follows. By the Euler-Lagrange equation the bosons' EOM are given by $\phi^a = \frac{i}{(q-1)!} C^a_{j_1 \ldots j_{q-1}} \psi_{j_1} \cdots \psi_{j_{q-1}}$. Inserting this into the SYK* Hamiltonian eq. (3.1) one obtains

$$H = \frac{1}{2} \frac{1}{(q-1)!^2} C^a_{i_1 \ldots i_{q-1}} C^a_{j_1 \ldots j_{q-1}} \psi_{i_1} \cdots \psi_{i_{q-1}} \psi_{j_1} \cdots \psi_{j_{q-1}}. \tag{3.6}$$

This is effectively the same as the SYK Hamiltonian eq. (2.1) but with a $(2q-2)$-point instead of a q-point interaction and with altered disorder-average statistics. In fact, SYK* and SYK are related by a Hubbard-Stratonovich transformation on the couplings given (for $q = 3$) by [25]

$$J_{ijkl} = -\frac{1}{8} \sum_{a=1}^{M} C^a_{[ij} C^a_{kl]}, \tag{3.7}$$

where $[\cdot]$ represents all possible anti-symmetric permutations. We have explicitly written the sum over index a to avoid confusion. This implies that the couplings J_{ijkl} are no longer independent Gaussian random variables but are related by the above transformation.

Although the SYK* model is able to nearly recreate the SYK model, it is intrinsically different from SYK as the following example illustrates. Consider the diagrams in fig. 3.2a ($q = 4$, SYK) and fig. 3.2b ($q = 3$, SYK*). These two

(a) (b)

Figure 3.2: A J^3-order correction to the fermionic propagator in SYK and SYK*. Dashed lines in fig. 3.2a cannot connect vertices pairwise so the result vanishes. By contrast, the "equivalent" SYK* diagram in fig. 3.2b is non-vanishing.

diagrams are considered "equivalent" because after integrating away the bosons the latter resembles the former. It is clear that the first is 0 due to disorder averaging over an odd number of vertices. Meanwhile, the second is equal to $2J^3\sqrt{\frac{N}{M}}$, which for large N and M but fixed $\frac{N}{M}$ is a nonzero contribution to the 1PI fermionic self-energy. This goes to show that the SYK* model consists of a broader class of diagrams than the SYK model, and so are inherently distinct.

3.2 Effective action

In chapter 2 we deduced the SYK self-energy using that all non-vanishing diagrams at large N were melons. In this section we will determine the fermionic and bosonic self-energies of SYK* via an alternative, more formal approach: the saddle point method. We reiterate that the following derivation heavily relies on the assumption of replica diagonal matrices discussed in subsection 2.2.2.

3.2.1 Integral over the disorder

In this subsection we denote the indices $i_1 \dots i_{q-1}$ as one collective index I in the interest of legibility. The first step is to integrate the partition function over the random disorder. That is, we must calculate

$$\langle Z\rangle_{\mathrm{D}} = \int \mathrm{D}[\psi]\,\mathrm{D}[\phi]\,\mathrm{D}[C_I^a] P(C_I^a) e^{-S_\psi - S_\phi - S_1}, \tag{3.8}$$

$$S_\psi = \int \mathrm{d}\tau \Big(\frac{1}{2}\psi_i \dot{\psi}_i\Big), \quad S_\phi = \int \mathrm{d}\tau \Big(-\frac{1}{2}\phi^a\phi^a\Big), \tag{3.9}$$

$$S_1 = \int \mathrm{d}\tau \frac{i}{(q-1)!} C_I^a \phi^a \psi_I, \tag{3.10}$$

where ψ_I is short for $\psi_{i_1}\cdots\psi_{i_{q-1}}$. The normalized Gaussian probability density function is of course

$$P(C_I^a) = \frac{1}{\sqrt{2\pi\sigma^2}} e^{-\frac{(C_I^a)^2}{2\sigma^2}} \quad \text{with} \quad \sigma^2 = \frac{(q-1)!J}{N^{q-3/2}M^{1/2}}. \tag{3.11}$$

We can then write eq. (3.8) as

$$\langle Z\rangle_{\mathrm{D}} = \int \mathrm{D}[\psi]\,\mathrm{D}[\phi]\,\mathrm{D}[C_I^a] \frac{1}{\sqrt{2\pi\sigma^2}} \exp\left[-\frac{1}{2\sigma^2}(C_I^a)^2 + B_I^a C_I^a - S_\psi - S_\phi\right] \tag{3.12}$$

where we have defined

$$B_I^a = \frac{-i}{(q-1)!} \int \mathrm{d}\tau \Big(\phi^a \psi_I\Big), \tag{3.13}$$

Since eq. (3.12) is Gaussian in C_I^a we can readily integrate over the disorder average through a generalized version of the famous identity

$$\int_{\mathbb{R}} \mathrm{d}x e^{-ax^2+bx+c} = \sqrt{\frac{\pi}{a}} e^{\frac{b^2}{4a}+c}. \tag{3.14}$$

This yields

$$\langle Z \rangle_{\mathrm{D}} = \int \mathrm{D}[\psi]\,\mathrm{D}[\phi] \exp\left[\frac{\sigma^2}{2} B_I^a B_I^a - S_\psi - S_\phi\right]. \tag{3.15}$$

Using that

$$B_I^a B_I^a \equiv \sum_{a=1}^{M}\sum_{I=1}^{N} B_I^a B_I^a = (q-1)! \sum_{a=1}^{M} \sum_{1\le i_1<\ldots<i_{q-1}\le N} B_I^a B_I^a,$$

and anti-commuting the fermions, we can write out eq. (3.15) as

$$\langle Z \rangle_{\mathrm{D}} = \int \mathrm{D}[\psi]\,\mathrm{D}[\phi] \exp\left[-\int \mathrm{d}\tau \Big(\frac{1}{2}\psi_i\dot{\psi}_i - \frac{1}{2}\phi^a\phi^a\Big)\right] \exp\left[\frac{J/2}{N^{q-3/2}M^{1/2}} \int \mathrm{d}\tau_1\,\mathrm{d}\tau_2 \left(\phi^a(\tau_1)\phi^a(\tau_2)\psi_{i_1}(\tau_1)\psi_{i_1}(\tau_2)\cdots\psi_{i_{q-1}}(\tau_1)\psi_{i_{q-1}}(\tau_2)\right)\right]. \tag{3.16}$$

This is the effective action resulting from integrating out the disorder.

3.2.2 Bilocal fields

The effective action eq. (3.16) can be rewritten in terms of bilocal fields. This is done by introducing the fermionic and bosonic 'Green's functions',

$$\begin{aligned} G_\psi(\tau,\tau') &= \frac{1}{N}\psi_i(\tau)\psi_i(\tau'), \\ G_\phi(\tau,\tau') &= \frac{1}{M}\phi^a(\tau)\phi^a(\tau'), \end{aligned} \tag{3.17}$$

and 'self-energy' bilocals (Lagrange multipliers setting eq. (3.17)),

$$1 = \int \mathrm{D}[G_\psi]\,\mathrm{D}[\Sigma_\psi] e^{-\frac{N}{2}\Sigma_\psi(\tau,\tau')\left[G_\psi(\tau,\tau') - \frac{1}{N}\psi_i(\tau)\psi_i(\tau')\right]}, \tag{3.18}$$

$$1 = \int \mathrm{D}[G_\phi]\,\mathrm{D}[\Sigma_\phi] e^{-\frac{M}{2}\Sigma_\phi(\tau,\tau')\left[G_\phi(\tau,\tau') - \frac{1}{M}\phi^a(\tau)\phi^a(\tau')\right]}. \tag{3.19}$$

Ultimately in the large N and M limit, these will coincide exactly with the fermionic and bosonic Green's functions and self-energies. Inserting these into the path

integral in eq. (3.16) gives

$$\langle Z\rangle_{\mathrm{D}} = \int \mathrm{D}[\psi]\,\mathrm{D}[\phi]\,\mathrm{D}[G_\psi]\cdots\mathrm{D}[\Sigma_\phi]\exp\Bigg[-\int \mathrm{d}\tau\Big(\frac{1}{2}\psi_i\dot{\psi}_i - \frac{1}{2}\phi^a\phi^a\Big)$$
$$+\frac{J/2}{N^{q-3/2}M^{1/2}}\int \mathrm{d}\tau_1\,\mathrm{d}\tau_2\Big(\phi^a(\tau_1)\phi^a(\tau_2)\psi_{i_1}(\tau_1)\psi_{i_1}(\tau_2)\cdots\psi_{i_{q-1}}(\tau_1)\psi_{i_{q-1}}(\tau_2)\Big)$$
$$+\int \mathrm{d}\tau_1\,\mathrm{d}\tau_2\Big(-\frac{N}{2}\Sigma_\psi(\tau_1,\tau_2)G_\psi(\tau_1,\tau_2)+\frac{1}{2}\Sigma_\psi(\tau_1,\tau_2)\psi_i(\tau_1)\psi_i(\tau_2)$$
$$-\frac{M}{2}\Sigma_\phi(\tau_1,\tau_2)G_\psi(\tau_1,\tau_2)+\frac{1}{2}\Sigma_\phi(\tau_1,\tau_2)\phi^a(\tau_1)\phi^a(\tau_2)\Big)\Bigg]. \quad (3.20)$$

Using eq. (3.17), the above can be written as

$$\langle Z\rangle_{\mathrm{D}} = \int \mathrm{D}[\psi]\,\mathrm{D}[\phi]\,\mathrm{D}[G_\psi]\cdots\mathrm{D}[\Sigma_\phi]$$
$$\exp\Bigg\{-\int \mathrm{d}\tau_1\,\mathrm{d}\tau_2\Big[\frac{1}{2}\psi_i(\tau_1)\Big(\delta(\tau_1-\tau_2)\partial_\tau-\Sigma_\psi(\tau_1,\tau_2)\Big)\psi_i(\tau_2)\Big]$$
$$-\int \mathrm{d}\tau_1\,\mathrm{d}\tau_2\Big[\frac{1}{2}\phi^a(\tau_1)\Big(-\delta(\tau_1-\tau_2)-\Sigma_\phi(\tau_1,\tau_2)\Big)\phi^a(\tau_2)\Big]$$
$$+\int \mathrm{d}\tau_1\,\mathrm{d}\tau_2\Big[\frac{J}{2}\sqrt{NM}G_\phi(\tau_1,\tau_2)G_\psi(\tau_1,\tau_2)^{q-1}-\frac{N}{2}\Sigma_\psi(\tau_1,\tau_2)G_\psi(\tau_1,\tau_2)$$
$$-\frac{M}{2}\Sigma_\phi(\tau_1,\tau_2)G_\phi(\tau_1,\tau_2)\Big]\Bigg\}. \quad (3.21)$$

This leaves us with path integrals over local Gaussian fields $\psi(\tau)$ and $\phi(\tau)$, and over bilocal fields $G_\psi(\tau,\tau')$, $\Sigma_\psi(\tau,\tau')$, $G_\phi(\tau,\tau')$, and $\Sigma_\phi(\tau,\tau')$.

3.2.3 Integral over local fields

Equation (3.21) can be further simplified by integrating away the local Gaussian functions. Doing this yields,

$$\langle Z\rangle_{\mathrm{D}} = \int \mathrm{D}[G_\psi]\cdots\mathrm{D}[\Sigma_\phi]\sqrt{\frac{\det[\delta(\tau_1-\tau_2)\partial_\tau-\Sigma_\psi(\tau_1,\tau_2)]^N}{\det[-\delta(\tau_1-\tau_2)-\Sigma_\phi(\tau_1,\tau_2)]^M}}$$
$$\exp\Bigg\{N\int \mathrm{d}\tau_1\,\mathrm{d}\tau_2\Big[\frac{J}{2}\sqrt{\frac{M}{N}}G_\phi(\tau_1,\tau_2)G_\psi(\tau_1,\tau_2)^{q-1}-\frac{1}{2}\Sigma_\psi(\tau_1,\tau_2)G_\psi(\tau_1,\tau_2)$$
$$-\frac{M}{2N}\Sigma_\phi(\tau_1,\tau_2)G_\phi(\tau_1,\tau_2)\Big]\Bigg\}. \quad (3.22)$$

The determinants are the result of evaluating Gaussian integrals over complex and Grassmannian fields. Using that $e^{\frac{1}{2}\mathrm{Tr}[\log(A)]} = \mathrm{Pf}(A)$, the Pfaffian of A, and $\det(\dots)^{\frac{1}{2}} = e^{\frac{1}{2}\log[\det(\dots)]}$ to rewrite eq. (3.22) as

$$\begin{aligned}\langle Z\rangle_{\mathrm{D}} = \int \mathrm{D}[G_\psi]\cdots\mathrm{D}[\Sigma_\phi] \\ \exp\Bigg\{N\int \mathrm{d}\tau_1\,\mathrm{d}\tau_2\Bigg[\frac{J}{2}\sqrt{\frac{M}{N}}G_\phi(\tau_1,\tau_2)G_\psi(\tau_1,\tau_2)^{q-1} \\ -\frac{1}{2}\Sigma_\psi(\tau_1,\tau_2)G_\psi(\tau_1,\tau_2)-\frac{M}{2N}\Sigma_\phi(\tau_1,\tau_2)G_\phi(\tau_1,\tau_2)\Bigg]\Bigg\} \\ \exp\Bigg\{N\log\Bigg[\mathrm{Pf}\Big(\delta(\tau_1-\tau_2)\partial_\tau-\Sigma_\psi(\tau_1,\tau_2)\Big)\Bigg] \\ -\frac{M}{2}\log\Bigg[\det\Big(-\delta(\mathrm{tan}_1-\mathrm{tan}_2)-\Sigma_\phi(\tau_1,\tau_2)\Big)\Bigg]\Bigg\}. \end{aligned} \tag{3.23}$$

Thus we have found an effective action of SYK* solely in terms of the bilocal fields:

$$\langle Z\rangle_{\mathrm{D}} = \int \mathrm{D}[G_\psi]\cdots\mathrm{D}[\Sigma_\phi]e^{-NS_{\mathrm{Eff}}} \tag{3.24}$$

where

$$\begin{aligned}S_{\mathrm{Eff}} = -\log\Bigg[\mathrm{Pf}\Big(\delta(\tau_1-\tau_2)\partial_\tau-\Sigma_\psi(\tau_1,\tau_2)\Big)\Bigg] \\ +\frac{M}{2N}\log\Bigg[\det\Big(-\delta(\tau_1-\tau_2)-\Sigma_\phi(\tau_1,\tau_2)\Big)\Bigg] \\ -\int \mathrm{d}\tau_1\,\mathrm{d}\tau_2\Bigg[\frac{J}{2}\sqrt{\frac{M}{N}}G_\phi(\tau_1,\tau_2)G_\psi(\tau_1,\tau_2)^{q-1} \\ -\frac{1}{2}\Sigma_\psi(\tau_1,\tau_2)G_\psi(\tau_1,\tau_2)-\frac{M}{2N}\Sigma_\phi(\tau_1,\tau_2)G_\phi(\tau_1,\tau_2)\Bigg]. \end{aligned} \tag{3.25}$$

It is apparent that for $N \gg 1$, eq. (3.25) reduces to a classical action. By varying the above effective action with respect to G_ψ and G_ϕ yields the fermionic and bosonic saddle point equations of SYK*:

$$\Sigma_\psi(\tau,\tau') = (q-1)J\sqrt{\frac{M}{N}}G_\phi(\tau,\tau')G_\psi(\tau,\tau')^{q-2}, \tag{3.26}$$

$$\Sigma_\phi(\tau,\tau') = J\sqrt{\frac{N}{M}}G_\phi(\tau,\tau')^{q-1}. \tag{3.27}$$

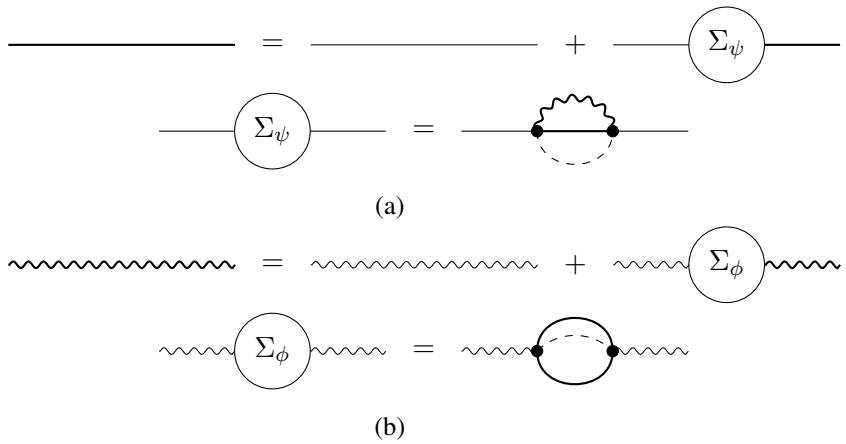

Figure 3.3: The Schwinger-Dyson recursion relation in SYK* for (a) fermions and (b) bosons. The thick straight (wiggly) lines denotes the dressed fermion (boson) propagators; the thin straight (wiggly) lines corresponds to the bare fermion (boson) propagator. The dashed line, as before, is the disorder averaging between two vertices.

These correctly reduce to the saddles initially found by Marcus and Vandoren for $q = 3$. Figure 3.3 depict the graphical representation of the resultant SD recursion relation. In the following section, we derive the SYK* conformal solutions in the IR limit based on these saddles.

3.2.4 Two branches

An important difference between the original SYK and SYK* is that the latter hosts two branches of conformal solutions, a rational and an irrational branch. We now review this result initially found by Marcus and Vandoren [25]. The reasoning will closely follow that of the original authors; we will work with $q = 3$ for simplicity.

Varying the effective action eq. (3.25) with respect to Σ_ψ and Σ_ϕ provides the SD equations (here given in frequency space):

$$G_\psi^{-1} = -i\omega_n - \Sigma_\psi \quad \text{and} \quad G_\phi^{-1} = -1 - \Sigma_\phi. \tag{3.28}$$

As with the SYK model, these equations are solvable for the Green's functions in the strong coupling limit, $N, M \gg \beta J \gg 1$. We see that the non-interacting Green's functions become negligible compared to the self-energies. We are there-

fore entitled to write (in Euclidean time)

$$-\delta(\tau-\tau') = \int d\tilde{\tau} G_\psi(\tau,\tilde{\tau})\Sigma_\psi(\tilde{\tau},\tau') \tag{3.29}$$

$$= 2J\sqrt{\frac{M}{N}}\int d\tilde{\tau} G_\psi(\tau,\tilde{\tau})G_\phi(\tilde{\tau},\tau')G_\psi(\tilde{\tau},\tau') \tag{3.30}$$

and

$$-\delta(\tau-\tau') = \int d\tilde{\tau} G_\phi(\tau,\tilde{\tau})\Sigma_\phi(\tilde{\tau},\tau') \tag{3.31}$$

$$= J\sqrt{\frac{N}{M}}\int d\tilde{\tau} G_\phi(\tau,\tilde{\tau})G_\psi(\tilde{\tau},\tau')^2. \tag{3.32}$$

These integral equations are conformally invariant at $T=0$ so that we can employ the fermionic and bosonic conformal ansatz,

$$G_\psi(\tau,0) = A\frac{\mathrm{sgn}(\tau)}{|\tau|^{2\Delta_\psi}} \quad \text{and} \quad G_\phi(\tau,0) = B\frac{1}{|\tau|^{2\Delta_\phi}}, \tag{3.33}$$

where the sign function is absent in $G_\phi(\tau,0)$ to make it even. Time-translation invariance was again used here. We can show that the SYK* conformal forms obey the correct symmetry properties of the fermionic and bosonic Green's functions in frequency space. To see this, we first Fourier transform eq. (3.33). This gives

$$G_\psi(i\omega_n) = -2iA\cos(\pi\Delta_\psi)\Gamma(1-2\Delta_\psi)\,\mathrm{sgn}(\omega_n)|\omega_n|^{2\Delta_\psi-1} \tag{3.34}$$

and

$$G_\phi(i\omega_n) = 2B\sin(\pi\Delta_\phi)\Gamma(1-2\Delta_\phi)|\omega_n|^{2\Delta_\phi-1} \tag{3.35}$$

We can then rewrite eq. (3.34) as

$$\begin{aligned} G_\psi(i\omega_n) &= A\Gamma(1-2\Delta_\psi)(e^{i\pi\Delta_\psi}+e^{-i\pi\Delta_\psi})|\omega_n|^{2\Delta_\psi}(i\omega_n)^{-1} \\ &= A\Gamma(1-2\Delta_\psi)[(e^{\frac{i\pi}{2}}|\omega_n|)^{2\Delta_\psi}+(e^{-i\frac{\pi}{2}}|\omega_n|)^{2\Delta_\psi}](i\omega_n)^{-1} \\ &= A\Gamma(1-2\Delta_\psi)[(i\omega_n)^{2\Delta_\psi}+(-i\omega_n)^{2\Delta_\psi}](i\omega_n)^{-1}, \end{aligned} \tag{3.36}$$

where we considered $\omega_n>0$ and $\omega_n<0$ separately to get the last line. It is clear that the fermionic Green's function is odd in frequency, i.e., $G_\psi(-i\omega_n) = -G_\psi(i\omega_n)$. Equation (3.35) can be rewritten as

$$\begin{aligned} G_\phi(i\omega_n) &= B\Gamma(1-2\Delta_\phi)(e^{i\pi\Delta_\phi}-e^{-i\pi\Delta_\phi})|\omega_n|^{2\Delta_\phi}(i|\omega_n|)^{-1} \\ &= B\Gamma(1-2\Delta_\phi)[(e^{\frac{i\pi}{2}}|\omega_n|)^{2\Delta_\phi}-(e^{-i\frac{\pi}{2}}|\omega_n|)^{2\Delta_\phi}](i|\omega_n|)^{-1} \\ &= B\Gamma(1-2\Delta_\phi)[(i\omega_n)^{2\Delta_\phi}-(-i\omega_n)^{2\Delta_\phi}](i\omega_n)^{-1}, \end{aligned} \tag{3.37}$$

where again the options $\omega_n>0$ and $\omega_n<0$ were considered separately in the last line. It is plain to see that the bosonic Green's function is even in frequency, i.e.,

$G_\phi(-i\omega_n) = G_\phi(i\omega_n)$.

Inserting eq. (3.34) and eq. (3.35) into the frequency space versions of eq. (3.29) and eq. (3.31) respectively and using properties of the Γ-function as we did previously, we obtain the following set of equations

$$\begin{aligned} 1 &= A^2 B \sqrt{\frac{M}{N}} \frac{4\pi J}{1-2\Delta_\psi} \frac{\cos(\pi\Delta_\psi)}{\sin(\pi\Delta_\psi)} |\omega|^{2(2\Delta_\psi+\Delta_\phi)-2} \\ 1 &= A^2 B \sqrt{\frac{N}{M}} \frac{2\pi J}{1-4\Delta_\psi} \tan(2\pi\Delta_\psi) |\omega|^{2(2\Delta_\psi+\Delta_\phi)-2}. \end{aligned} \tag{3.38}$$

By power counting the frequency in both sides of the equation, we get a constraint on the conformal dimensions:

$$2\Delta_\psi + \Delta_\phi = 1. \tag{3.39}$$

Another constraint is found if we divide the second equation in eq. (3.38) by the first:

$$\frac{N}{M} \tan(\pi\Delta_\psi) \tan(2\pi\Delta_\psi) = \frac{2(1-4\Delta_\psi)}{1-2\Delta_\psi}. \tag{3.40}$$

By setting $\frac{M}{N} = 1$, we can plot both sides of the above constraint with the hope of finding values of Δ_ψ at which these two functions intersect (see fig. 3.4). There are two such points of intersection. Numerically, they are found to be $\Delta_\psi = \frac{1}{6}$ and $\Delta_\psi \approx 0.350585$, so there are two values of Δ_ψ that satisfy the constraint eq. (3.40). Therefore two conformal solutions arise when $M = N$. Using the

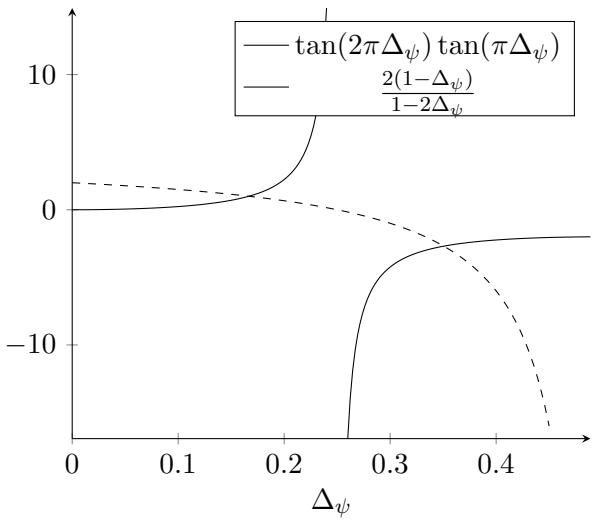

Figure 3.4: A plot showing both sides of the transcendental equation, eq. (3.40). There are two clear intersection points, at $\Delta_\psi = \frac{1}{6}$ and $\Delta_\psi \approx 0.350585$.

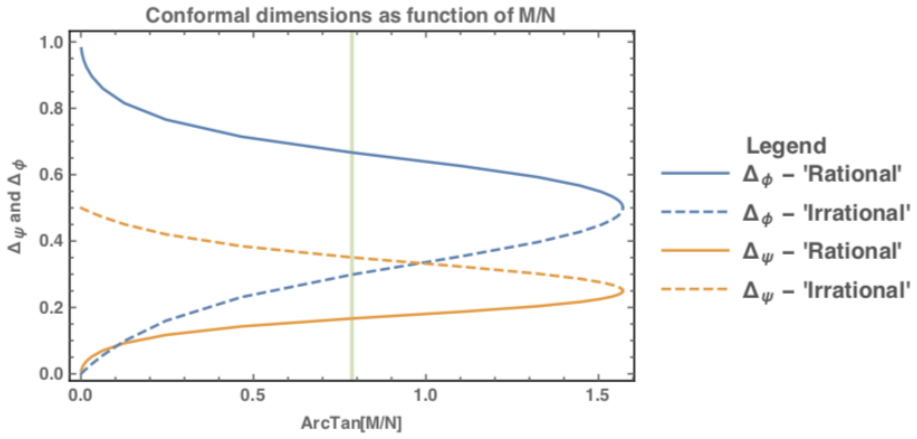

Figure 3.5: The conformal dimensions as a function of the ratio $\frac{M}{N}$. The figure is taken from section 3.1.2 of [25].

constraint eq. (3.39), we identify the first solution:

$$\Delta_\psi = \frac{1}{6}, \quad \Delta_\phi = \frac{2}{3}, \quad A^2 B = \frac{1}{6\pi J\sqrt{3}},. \tag{3.41}$$

This was referred to as the "rational" solution by the original authors. The other solution, called the "irrational" solution, is approximately given by

$$\Delta_\psi \approx 0.350585, \quad \Delta_\phi \approx 0.29881, \quad A^2 B \approx \frac{0.589161}{4\pi J}. \tag{3.42}$$

One issue with the SYK* conformal solutions is that there is as of yet no way of determining the constants A and B independently: only the combination $A^2 B$ is known. By letting the ratio $\frac{M}{N}$ vary, Marcus and Vandoren numerically found the conformal dimensions as a function of this parameter, shown in fig. 3.5. They showed that two branches or families of solutions arose for each conformal dimension, characterized by their "rationality" at $M = N$. By sending $\frac{M}{N} \gg 1$, it is seen (both from the figure and from eq. (3.40)) that the rational and irrational branches tend to the same solution, namely

$$\Delta_\psi = \frac{1}{4}, \quad \Delta_\phi = \frac{1}{2}, \quad A^2 B = \frac{1}{8\pi J\sqrt{\frac{M}{N}}}. \tag{3.43}$$

This is a significant limiting behavior since $\Delta_\psi = 1/4$ corresponds exactly to the IR conformal dimension in SYK.

3.2.5 Spectral functions

Given eq. (3.36) and eq. (3.37), it is not difficult to plot the fermionic and bosonic spectral functions for different conformal dimensions. These are simply

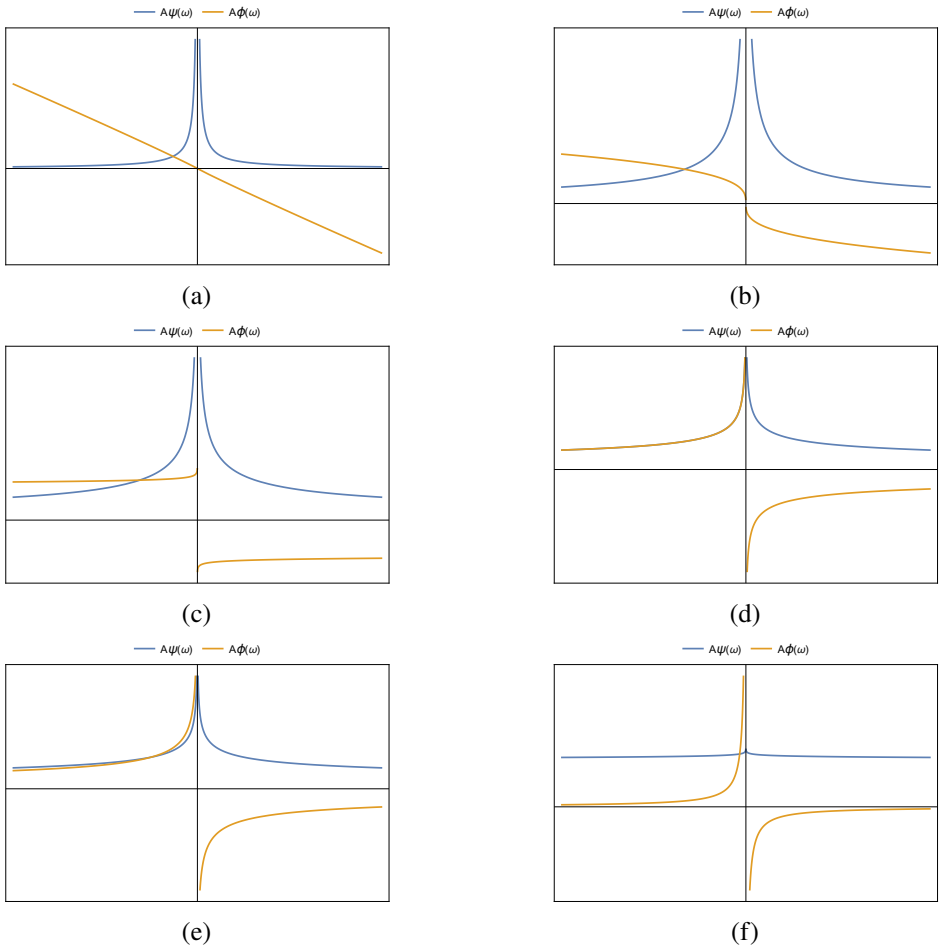

Figure 3.6: Fermionic (blue) and bosonic (orange) spectral functions for different conformal dimensions Δ_ψ and Δ_ϕ. Figures (a) through (f) have fermionic conformal dimension Δ_ψ ranging form (approximately) 0 to $1/2$ (see table 3.1). The bosonic conformal dimension follows from eq. (3.39). To produce the above plots, we needed to set values for the constants A and B. For simplicity we have set $A = B = 1$ though in general this may not be the case.

given by $A_{\psi,\phi}(\omega) \equiv -2\text{Im}[G^{\text{R}}_{\psi,\phi}(\omega)]$ where $G^{\text{R}}_{\psi,\phi}(\omega) = G_{\psi,\phi}(\omega + i\epsilon)$ denotes the retarded fermionic/bosonic Green's function. The spectral functions for various conformal dimensions are shown in fig. 3.6 (see table 3.1 for the association). In a non-interacting theory the spectral function is a δ-function, while in an interacting theory the nonzero imaginary part of the self-energy broadens the spectral function into a Gaussian bump. Here, however, we see that the fermionic and bosonic spectral weights are spread across all frequencies. Since the width of the spectra correspond to the inverse quasi-particle lifetime, the infinite width spectra shown have extremely short-lived quasi-particles. This supports the claim that SYK and

Subfigure	Conformal dimension	
(a)	$\Delta_\psi \approx 0$	$\Delta_\phi \approx 1$
(b)	$\Delta_\psi = 1/6$	$\Delta_\phi = 2/3$
(c)	$\Delta_\psi = 1/4$	$\Delta_\phi = 1/2$
(d)	$\Delta_\psi = 1/3$	$\Delta_\phi = 1/3$
(e)	$\Delta_\psi \approx 0.351$	$\Delta_\phi \approx 0.299$
(f)	$\Delta_\psi \approx 1/2$	$\Delta_\phi \approx 0$

Table 3.1: Conformal dimensions associated to the subfigures in fig. 3.6.

SYK-like models are "unparticle" theories; they do not exhibit quasi-particle excitations.[2]

The above families of conformal solution hold true in the limit of strong coupling, $N \gg \beta J \gg 1$, in which the conformal ansatz played a crucial role. One can, however, pose a similar but different question: what do we find if we consider the $\frac{M}{N} \gg 1$ and $\frac{M}{N} \ll 1$ regimes at fixed coupling constant J? While we cannot use the conformal form of the Green's functions, the saddle point equations found in section 3.2 simplify in the large and small $\frac{M}{N}$ regimes. We will explore this parameter space in chapter 4. Before that though, we shortly comment on the strange affinity between SYK* and a theory of holographic fermions.

3.3 SYK* and holographic fermions

In this section, we briefly draw a passing resemblance between the SYK* model and a model of semi-holographic fermions (SHF) [32]. At first sight, there is no evidence to suggest a connection between these two models. The SHF theory is a theory of Dirac fermions living in $3+1$ dimensions coupled to a CFT. They originate as chiral Dirac fermions in $4+1$ dimensional AdS spacetime with a planar Schwarzchild black hole. After integrating out the CFT (*inter alias*), one finds a retarded Green's function for Dirac fermions with self-energy representing the interaction with the strongly coupled CFT:

$$G^{\mathrm{R}}_{\mathrm{SHF}}(\omega) \propto [-(\omega + i\epsilon)^2]^{\frac{1}{2}-M}(\omega + i\epsilon)^{-1}, \tag{3.44}$$

where $-\frac{1}{2} < M < \frac{1}{2}$ is the dimensionless bulk Dirac mass. In the boundary field theory, this becomes a model parameter (the conformal dimension). Meanwhile the (fermionic) retarded Green's function in SYK* was found above to be:

$$G^{\mathrm{R}}_{\mathrm{SYK}^*}(\omega) \propto [(\omega + i\epsilon)^{2\Delta} + (-\omega - i\epsilon)^{2\Delta}](\omega + i\epsilon)^{-1}. \tag{3.45}$$

[2]In the exceptional case $\Delta_\psi = 0$, the fermions are free: the fermionic spectral function becomes a δ-function. Similarly, $\Delta_\phi = 0$ means the bosons are non-interacting so their spectral functions also become a well-localized peaks.

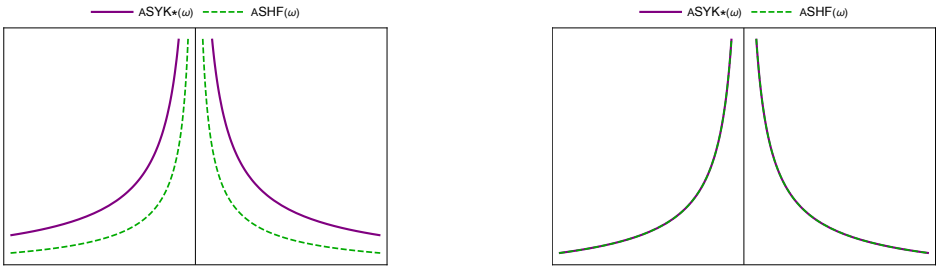

(a) (b)

Figure 3.7: Comparison of fermionic spectra in SYK* and SHF. The solid purple line denotes the fermionic spectral function in SYK*, $A_{\text{SYK}^*}(\omega)$; the dashed green line is that of SHF, $A_{\text{SHF}}(\omega)$. In (b), $A_{\text{SHF}}(\omega)$ was rescaled by eq. (3.49).

In order to compare eq. (3.44) and eq. (3.45), we must identify their conformal dimensions. This is done by seeing how the respective Green's functions transform under the rescaling $\omega \to \lambda\omega$. We get that

$$G_{\text{SYK}^*}(\omega) \longrightarrow \lambda^{2\Delta_\psi - 1} G_{\text{SYK}^*}(\omega) \tag{3.46}$$

while

$$G_{\text{SHF}}(\omega) \longrightarrow \lambda^{-2M} G_{\text{SHF}}(\omega). \tag{3.47}$$

By matching the scaling behavior, we obtain the relation $2\Delta_\psi - 1 = -2M$, or,

$$\Delta_\psi + M = \frac{1}{2}, \tag{3.48}$$

implying that $0 < \Delta_\psi < 1$. Let us select $\Delta_\psi = \frac{1}{8}$ and $M = \frac{3}{8}$, for instance. The two models' spectral functions are plotted in fig. 3.7, from which we see a striking resemblance: the fermionic spectra of SYK* and of SHF (fig. 3.7a) are equal to each other (fig. 3.7b) up to a factor. By writing $\pm(\omega + i\epsilon)$ in eq. (3.44) and eq. (3.45) in polar form, the factor can be found exactly:

$$\frac{G^{\text{R}}_{\text{SYK}^*}}{G^{\text{R}}_{\text{SHF}}} = \frac{\sin\left(\frac{\pi}{4}\right)}{\sin\left(\frac{\pi}{8}\right)}. \tag{3.49}$$

This project did not succeed in elucidating the nature of this unexpected connection. In retrospect the perfect coincidence of the SYK* and SHF spectra is a direct result of fixing the conformal dimensions Δ_ψ and M through eq. (3.48). However at a more fundamental level, it is not understood how a model of $0+1$ dimensional highly entangled Majorana fermions and a $3+1$ dimensional theory of Dirac spinors in curved spacetime can describe the same underlying physics.

Chapter 4

$\frac{M}{N}$ Parameter space

In this chapter we discuss the possible self-consistent solutions to the Green's functions and self energies that arise in the regimes $\frac{M}{N} \gg 1$ and $\frac{M}{N} \ll 1$ of the SYK* model. Here the coupling strength J is kept fixed at finite value, unlike in the SYK model where the $J \to \infty$ limit was needed to proceed analytically. In studying these regimes we will encounter an intriguing result: a critical boundary in the phase space of the $T - \frac{M}{N}$ plane arises. As the fermionic and bosonic self energies previously found in section 3.2 are the starting point of this analysis, we remind them here:

$$\begin{aligned} \Sigma_\psi(\tau,\tau') &= (q-1)J\sqrt{\frac{M}{N}}G_\phi(\tau,\tau')G_\psi(\tau,\tau')^{q-2} \\ \Sigma_\phi(\tau,\tau') &= J\sqrt{\frac{N}{M}}G_\psi(\tau,\tau')^{q-1}. \end{aligned} \tag{4.1}$$

In what follows, we will use superscripts B and F to differentiate between even and odd Matsubara frequencies.

4.1 The $\frac{M}{N} \gg 1$ regime

Let us begin by considering the $\frac{M}{N} \gg 1$ regime (see fig. 4.1). In it, the bosonic self energy in eq. (4.1) becomes negligible while the fermionic self-energy dominates. As a result, the dressed bosonic propagator may be approximated by

$$G_\phi = \frac{1}{(G_\phi^0)^{-1} - \Sigma_\phi} \approx G_\phi^0. \tag{4.2}$$

Based on this observation, we consider an effective theory in which bosons are free. Under this assumption we can self-consistently solve for the fermionic Green's

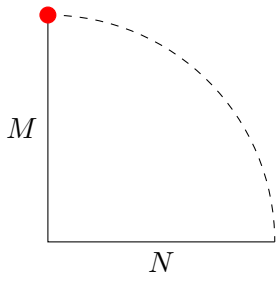

Figure 4.1: A compactified depiction of the parameter space of SYK* for M bosons and N fermions. The dashed line denotes the large M and N limits. In this section we probe the $\frac{M}{N} \gg 1$ regime indicated by the red dot.

function. To do so, we begin by expanding eq. (4.1) in Matsubara frequencies as

$$\Sigma_\psi(i\Omega_n^{\mathrm{F}}) = (q-1)J\sqrt{\frac{M}{N}}\frac{1}{\beta^{q-2}}\sum_{n'\in\mathbb{Z}}\sum_{n_2''\in\mathbb{Z}}\cdots\sum_{n_{q-2}''\in\mathbb{Z}} G_\phi(i\omega_{n'}^{\mathrm{B}})$$
$$G_\psi(i\Omega_n^{\mathrm{F}} - i\omega_{n_2''}^{\mathrm{F}} - \ldots - i\omega_{n_{q-2}''}^{\mathrm{F}} - i\omega_{n'}^{\mathrm{B}})G_\psi(i\omega_{n_2''}^{\mathrm{F}})\cdots G_\psi(i\omega_{n_{q-2}''}^{\mathrm{F}}). \quad (4.3)$$

By our assumption, we have that $G_\phi = G_\phi^0 = -1$ so by substituting in the SD equation for the fermionic Green's functions we get

$$\Sigma_\psi(i\Omega_n^{\mathrm{F}}) = -(q-1)J\sqrt{\frac{M}{N}}\frac{1}{\beta^{q-2}}\sum_{n'\in\mathbb{Z}}\sum_{n_2''\in\mathbb{Z}}\cdots\sum_{n_{q-2}''\in\mathbb{Z}}$$
$$\frac{1}{-i\Omega_n^F + i\omega_{n_2''}^{\mathrm{F}} + \ldots + i\omega_{n_{q-2}''}^{\mathrm{F}} + i\omega_{n'}^{\mathrm{B}} - \Sigma_\psi(i\Omega_n^{\mathrm{F}} - i\omega_{n_2''}^{\mathrm{F}} - \ldots - i\omega_{n_{q-2}''}^{\mathrm{F}} - i\omega_{n'}^{\mathrm{B}})}$$
$$\frac{1}{-i\omega_{n_2''}^{\mathrm{F}} - \Sigma_\psi(i\omega_{n_2''}^{\mathrm{F}})}\cdots\frac{1}{-i\omega_{n_{q-2}''}^{\mathrm{F}} - \Sigma_\psi(i\omega_{n_{q-2}''}^{\mathrm{F}})}. \quad (4.4)$$

As it stands, the above equation is intractable since we do not *a priori* know the explicit frequency dependence of Σ_ψ. However one can show that

$$\Sigma_\psi(i\Omega_n^{\mathrm{F}} - i\omega_{m_2''}^{\mathrm{F}} - \ldots - i\omega_{m_{q-2}''}^{\mathrm{F}} - i\omega_{m'}^{\mathrm{B}}) = \Sigma_\psi(i\Omega_n^{\mathrm{F}}) \quad (4.5)$$

for any fermionic and bosonic Matsubara frequencies indexed by m_2'', …, m_{q-2}'' and m', respectively. We can easily demonstrate this by writing out the left-hand side of eq. (4.5) using eq. (4.4):

$$\Sigma_\psi(i\Omega_n^{\mathrm{F}} - i\omega_{m_2''}^{\mathrm{F}} - \ldots - i\omega_{m_{q-2}''}^{\mathrm{F}} - i\omega_{m'}^{\mathrm{B}}) = -(q-1)J\sqrt{\frac{M}{N}}\frac{1}{\beta^{q-2}}\sum_{n'\in\mathbb{Z}}\sum_{n_2''\in\mathbb{Z}}\cdots$$
$$\sum_{n_{q-2}''\in\mathbb{Z}}\frac{1}{-i\Omega - \Sigma_\psi(i\Omega)}\frac{1}{-i\omega_{n_2''}^{\mathrm{F}} - \Sigma_\psi(i\omega_{n_2''}^{\mathrm{F}})}\cdots\frac{1}{-i\omega_{n_{q-2}''}^{\mathrm{F}} - \Sigma_\psi(i\omega_{n_{q-2}''}^{\mathrm{F}})}, \quad (4.6)$$

where we have introduced the shorthand $\Omega = \Omega_n^{\mathrm{F}} - \omega_{m_2''}^{\mathrm{F}} - \ldots - \omega_{m_{q-2}''}^{\mathrm{F}} - \omega_{m'}^{\mathrm{B}} - \omega_{n_2''}^{\mathrm{F}} - \ldots - \omega_{n_{q-2}''}^{\mathrm{F}} - \omega_{n'}^{\mathrm{B}}$. Since q must be odd, we have that $\omega_{m_2''}^{\mathrm{F}} + \ldots + \omega_{m_{q-2}''}^{\mathrm{F}}$ is a sum of an *even* number of fermionic Matsubara frequencies. This is necessarily equal to a bosonic Matsubara frequency. Therefore we can write our shorthand as

$$\Omega = \Omega_n^{\mathrm{F}} - \omega_m^{\mathrm{B}} - \omega_{m'}^{\mathrm{B}} - \omega_{n_2''}^{\mathrm{F}} - \ldots - \omega_{n_{q-2}''}^{\mathrm{F}} - \omega_{n'}^{\mathrm{B}}.$$

Now we use that the sum of two bosonic Matsubara frequencies is another bosonic Matsubara frequency to write

$$\Omega = \Omega_n^{\mathrm{F}} - \omega_{n_2''}^{\mathrm{F}} - \ldots - \omega_{n_{q-2}''}^{\mathrm{F}} - \omega_s^{\mathrm{B}}$$

where we have relabeled the sum over n' to one over s. Our shorthand has been reduced to precisely the terms appearing in eq. (4.4), thus it follows that eq. (4.5) is true.[1] So eq. (4.4) now reads

$$\Sigma_\psi(i\Omega_n^{\mathrm{F}}) = -(q-1)J\sqrt{\frac{M}{N}}\frac{1}{\beta^{q-2}}\sum_{n'\in\mathbb{Z}}\sum_{n_2''\in\mathbb{Z}}\cdots\sum_{n_{q-2}''\in\mathbb{Z}} \frac{1}{-i\Omega_n^{\mathrm{F}} + i\omega_{n_2''}^{\mathrm{F}} + \ldots + i\omega_{n_{q-2}''}^{\mathrm{F}} + i\omega_{n'}^{\mathrm{B}} - \Sigma_\psi(i\Omega_n^{\mathrm{F}})} \frac{1}{-i\omega_{n_2''}^{\mathrm{F}} - \Sigma_\psi(i\omega_{n_2''}^{\mathrm{F}})}\cdots\frac{1}{-i\omega_{n_{q-2}''}^{\mathrm{F}} - \Sigma_\psi(i\omega_{n_{q-2}''}^{\mathrm{F}})}. \quad (4.7)$$

Next, we can freely shift the frequencies $\omega_{n_i''}^{\mathrm{F}}$ to $\omega_{n_i''}^{\mathrm{B}} + \Omega_n^{\mathrm{F}}$ since they are summed over. This will produce $q-3$ additional occurences of $+i\Omega_n^{\mathrm{F}}$ in the denominator of the larger fraction, and one occurence of $-i\Omega_n^{\mathrm{F}}$ for each of the smaller fractions (with $\Sigma_\psi(i\omega_{n_i''}^{\mathrm{F}})$ going to $\Sigma_\psi(i\omega_{n_i''}^{\mathrm{B}} + \Omega_n^{\mathrm{F}})$. By using a simpler analogue of eq. (4.5), we rewrite eq. (4.7) as

$$\Sigma_\psi(i\Omega_n^{\mathrm{F}}) = -(q-1)J\sqrt{\frac{M}{N}}\frac{1}{\beta^{q-2}}\sum_{n'\in\mathbb{Z}}\sum_{n_2''\in\mathbb{Z}}\cdots\sum_{n_{q-2}''\in\mathbb{Z}} \frac{1}{-i\Omega_n^{\mathrm{F}} + i\omega_{n_2''}^{\mathrm{B}} + \ldots + i\omega_{n_{q-2}''}^{\mathrm{B}} + i\omega_{n'}^{\mathrm{B}} - \Sigma_\psi(i\Omega_n^{\mathrm{F}})} \frac{1}{-i\omega_{n_2''}^{\mathrm{B}} - i\Omega_n^{F} - \Sigma_\psi(i\Omega_n^{\mathrm{F}})}\cdots\frac{1}{-i\omega_{n_{q-2}''}^{\mathrm{B}} - i\Omega_n^{F} - \Sigma_\psi(i\Omega_n^{\mathrm{F}})}. \quad (4.8)$$

We are now in a position to evaluate the multiple Matsubara sums. Note that although the sums can be performed in any order, it is more straightforward to sum

[1] This identity can also be viewed simply as the result of shifting the momentum of virtual particles in loops.

over n' first since then the other sums will completely decouple. The main identity used in evaluation a Matsubara sum is

$$\frac{1}{\beta}\sum_{n\in\mathbb{Z}} \frac{-1}{i\omega_n^{\mathrm{B}} - A} = \frac{1}{e^{\beta A}-1} + \frac{1}{2} \tag{4.9}$$

where $\mathfrak{Re}(A) > 0$ (consult appendix A for details). Repeated use of eq. (4.9) in eq. (4.8) yields

$$\begin{aligned}\Sigma_\psi(i\Omega_n^{\mathrm{F}}) &= -(q-1)J\sqrt{\frac{M}{N}}\left(\frac{1}{e^{\beta\Sigma_\psi(i\Omega_n^{\mathrm{F}})}+1} - \frac{1}{2}\right)\left(\frac{1}{e^{-\beta\Sigma_\psi(i\Omega_n^{\mathrm{F}})}+1} - \frac{1}{2}\right)^{q-3} \\ &= -(q-1)J\sqrt{\frac{M}{N}}\left(\frac{1}{e^{\beta\Sigma_\psi(i\Omega_n^{\mathrm{F}})}+1} - \frac{1}{2}\right)^{q-2},\end{aligned} \tag{4.10}$$

where in the second line we used the fact that eq. (4.9) is odd under $A \to -A$ and that $q-3$ is even for odd q. By rescaling as $\Sigma_\psi \to J\sqrt{\frac{M}{N}}\Sigma_\psi$ and introducing the dimensionless variables $\lambda = \beta J\sqrt{\frac{M}{N}}$, we can write eq. (4.10) as

$$\Sigma_\psi(i\Omega_n^{\mathrm{F}}) = -(q-1)\left(\frac{1}{e^{\lambda\Sigma_\psi(i\Omega_n^{\mathrm{F}})}+1} - \frac{1}{2}\right)^{q-2}. \tag{4.11}$$

This form is practical since we can now plot both sides of eq. (4.11) as functions of Σ_ψ for different values of λ. This is shown in fig. 4.2. Solutions to eq. (4.11) correspond to the intersections between the solid line and dashed line in the figure. We see that there are essentially three such non-negative intersections. One of them is the trivial solution $\Sigma_\psi = 0$; then there are two others, the greater solution and the smaller solution.

The non-trivial solutions to eq. (4.10) (greater one and smaller one in fig. 4.2) can straightforwardly be found. For a fixed non-zero temperature and for large $\frac{M}{N}$ the greater one is

$$\Sigma_\psi(i\Omega_n^{\mathrm{F}}) = (q-1)J\sqrt{\frac{M}{N}}\Big(\frac{1}{2}\Big)^{q-2}\operatorname{sgn}(\Omega_n^{\mathrm{F}}). \tag{4.12}$$

Note that this is coincident with the zero-temperature ($\beta \to \infty$) limit of eq. (4.11). The smaller one can be found by expanding the right hand side of eq. (4.11) around the point $\Sigma_\psi = 0$. Doing this yields

$$\Sigma_\psi(i\Omega_n^{\mathrm{F}}) = (q-1)J\sqrt{\frac{M}{N}}\Big(\frac{\beta}{4}\Big)^{q-2}\Sigma_\psi(i\Omega_n^{\mathrm{F}})^{q-2}. \tag{4.13}$$

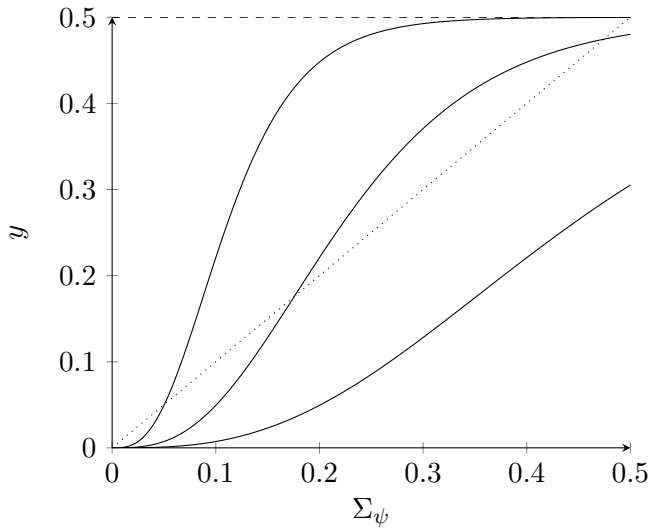

Figure 4.2: The self consistency equation eq. (4.11) plotted for $q = 5$. The dotted line depicts the curve $y = \Sigma_\psi$ while the solid line depicts the curve $y = -4[(e^{\lambda\Sigma_\psi} + 1)^{-1} - 1/2]^3$ for different values of $\lambda = \beta J\sqrt{\frac{M}{N}}$ ($\lambda = 20$, 10, and 5 from left to right). The dashed line corresponds to the large M/N limit.

This is solved by

$$\Sigma_\psi(i\Omega_n^{\mathrm{F}}) = \left[(q-1)J\sqrt{\frac{M}{N}}\left(\frac{\beta}{4}\right)^{q-2}\right]^{-\frac{1}{q-3}}, \tag{4.14}$$

which is sensible because in the limit of large $\frac{M}{N}$, the smaller solutions tends to $\Sigma_\psi = 0$.

At this point, let us pause the $\frac{M}{N}$ analysis to make a remark. An interesting question to ask is whether we observe any qualitative differences in SYK* if we consider the same model but with the sign-inverse coupling. This is a very relevant question in, for example, the Ising model of magnetism where the sign of the coupling J determines the system's ground state configuration (a ferromagnet when $J < 0$, an anti-ferromagnet when $J > 0$). In SYK* we cannot naively perform the change $J \to -J$ because this would tamper with the Gaussian disorder. Instead, we can change the sign of the bosons' mass, i.e., $\phi^a\phi^a \to -\phi^a\phi^a$. This effectively changes the sign of the interaction term in SYK* when the bosons are integrated out, as one can easily check. However, the consequence of this change is that the SYK* fermions become trivial in the $\frac{M}{N} \gg 1$ regime. This can be seen from fig. 4.3: the sign-change of the boson mass leads directly to the change $G_\phi^0 = -1 \to 1$ such that in the large $\frac{M}{N}$ limit only the trivial solution solves the altered eq. (4.11). That is, only $\Sigma_\psi = 0$ solves the sign-changed eq. (4.11).

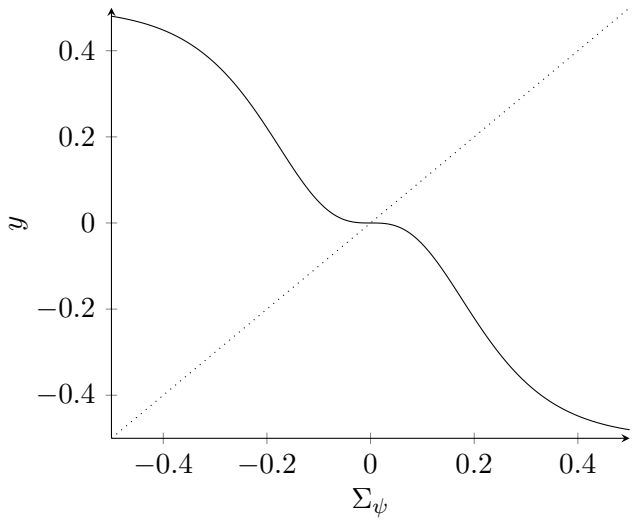

Figure 4.3: Upon changing the boson mass from $\phi^a\phi^a$ to $-\phi^a\phi^a$, SYK* becomes trivial in the large $\frac{M}{N}$ limit. The figure shows eq. (4.11) for $q = 5$: $y = 4[(e^{\lambda\Sigma_\psi} + 1)^{-1} - 1/2]^3$ (note the overall sign change) with $\lambda = 10$.

Let us now return to the $\frac{M}{N} \gg 1$ analysis. To validate eq. (4.10) and eq. (4.12) we must compute the boson self-energy using eq. (4.12) and ensure, as we have assumed in the above derivation, that it vanishes for large $\frac{M}{N}$. The boson self-energy is,

$$\Sigma_\phi(i\omega_n^{\mathrm{B}}) = J\sqrt{\frac{N}{M}}\frac{1}{\beta^{q-2}}\sum_{n_2''\in\mathbb{Z}}\cdots\sum_{n_{q-1}''\in\mathbb{Z}} G_\psi(i\omega_n^{\mathrm{B}} - i\omega_{n_2''}^{\mathrm{F}} - \ldots - i\omega_{n_{q-1}''}^{\mathrm{F}}) \\ G_\psi(i\omega_{n_2''}^{\mathrm{F}})\cdots G_\psi(i\omega_{n_{q-1}''}^{\mathrm{F}}). \quad (4.15)$$

The main identity we use now to evaluate the Matsubara sums is

$$\frac{1}{\beta}\sum_{n\in\mathbb{Z}}\frac{1}{i\omega_n^{\mathrm{B}} - A_1}\frac{-1}{i\omega_n^{\mathrm{B}} + A_2} = \left(\frac{1}{e^{\beta A_1} - 1} - \frac{1}{e^{-\beta A_2} - 1}\right)\frac{1}{A_1 + A_2}, \quad (4.16)$$

where $\mathfrak{Re}(A_1), \mathfrak{Re}(A_2) > 0$ (see appendix A). The boson self-energy is then given by

$$\Sigma_\phi(i\omega_n^{\mathrm{B}}) = 2J\sqrt{\frac{N}{M}}\frac{1}{(q-1)!}\frac{1}{i\omega_n^{\mathrm{B}} + (q-1)\Sigma_\psi(i\omega_n^{\mathrm{F}})} \\ \prod_{k=0}^{q-3}\left(\frac{1}{e^{-\beta\Sigma_\psi(i\omega_n^F)} + 1} + \frac{(-1)^{k+1}}{e^{(k+1)\beta\Sigma_\psi(i\omega_n^{\mathrm{F}})} + (-1)^k}\right), \quad (4.17)$$

from which we see that for fixed temperature and in the limit of large $\frac{M}{N}$, $\Sigma_\phi \to 0$ as it should.

To further verify the above results we can check that they are consistent with the saddles eq. (4.1) by transforming everything back to Euclidean time. This involves evaluating the Matsubara expansion

$$\begin{aligned} G_\psi(\tau) &= \frac{1}{\beta}\sum_n e^{-i\omega_n^{\mathrm{F}}\tau} G_\psi(i\omega_n^{\mathrm{F}}) \\ &= \frac{1}{\beta}\sum_n \frac{e^{-i\omega_n^{\mathrm{F}}\tau}}{-i\omega_n^{\mathrm{F}} - \Sigma_\psi(i\omega_n^{\mathrm{F}})}, \end{aligned} \tag{4.18}$$

where $\Sigma_\psi(i\omega_n^{\mathrm{F}})$ is as in eq. (4.12). This requires performing a contour integral in the presence of a branch cut along the $\mathbb{R}^-$ line. This integral has yet to be analytically worked out in full.

Besides the finite coupling solutions to the Green's function in the $\frac{M}{N} \gg 1$ regime, fig. 4.2 suggests something intriguing: there is a critical $\lambda = \beta J\sqrt{\frac{M}{N}}$, λ_c, at which the fermionic self energy goes from being zero-valued ($\lambda_c > \lambda$) to finite valued ($\lambda_c < \lambda$). We can attribute this to there being a critical temperature T within λ, T_c, signaling the presence of a phase transition. For $q = 3$, the critical temperature is analytically solvable and given by

$$T_c = \frac{J}{2}\sqrt{\frac{M}{N}}. \tag{4.19}$$

For $q > 3$, eq. (4.11) acquires an inflection point (as attested in fig. 4.2). This makes it difficult to find the critical temperature analytically. Numerically we can estimate T_c for given q:

$$q = 5 \qquad T_c \approx 0.124069J\sqrt{\tfrac{M}{N}}$$

$$q = 7 \qquad T_c \approx 0.039683J\sqrt{\tfrac{M}{N}}$$

$$q = 9 \qquad T_c \approx 0.012136J\sqrt{\tfrac{M}{N}}$$

Thus far, it is not immediately clear what two phases this transition is meant to be separating, nor the interpretation of the self energy as an order parameter governing the transition. To gain more insight on this transition we next explore the other corner of parameter space, the $\frac{M}{N} \ll 1$ regime.

4.2 The $\frac{M}{N} \ll 1$ regime

In this section we can probe the $\frac{M}{N} \ll 1$ regime (see fig. 4.4). Now the opposite happens: the bosonic self energy dominates while the fermionic self

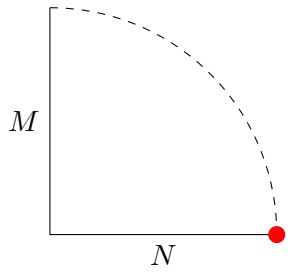

Figure 4.4: The regime of interest in the theory space of SYK* is now $\frac{M}{N} \ll 1$ for $M \gg 1$ and $N \gg 1$. This is indicated by the red point.

energy becomes negligible, i.e.,

$$G_\psi = \frac{1}{(G^0_\psi)^{-1} - \Sigma_\psi} \approx G^0_\psi. \tag{4.20}$$

In analogy with the previous section, we therefore assume an effective theory of free fermions and seek the self-consistent solution to the bosonic Green's function in this regime. We proceed in a similar way: performing a Matsubara expansion and using that $G_\psi = G^0_\psi = \frac{1}{-i\omega^{\mathrm{F}}_n}$ in the SD equation. This gives

$$\Sigma_\phi(i\omega^{\mathrm{B}}_n) = J\sqrt{\frac{N}{M}}\frac{1}{\beta^{q-2}}\sum_{n''_2}\cdots\sum_{n''_{q-1}} \frac{1}{-i\omega^{\mathrm{B}}_n + i\omega^{\mathrm{F}}_{n''_2} + \ldots + i\omega^{\mathrm{F}}_{n''_{q-1}}}\frac{1}{-i\omega^{\mathrm{F}}_{n''_2}}\cdots\frac{1}{-i\omega^{\mathrm{F}}_{n''_{q-1}}}. \tag{4.21}$$

There is a problem here however: the above Matsubara sums evaluate to 0 for finite ω^{B}_n (see appendix A). This is problematic if it is true for general ω^{B}_n because then SYK* would reduce to a trivial theory in the small $\frac{M}{N}$ limit. So let us check the result at zero-frequency: eq. (4.21) with $\omega^{\mathrm{B}}_n = 0$ is

$$\Sigma_\phi(0) = J\sqrt{\frac{N}{M}}\frac{1}{\beta^{q-2}}\sum_{n''_2}\cdots\sum_{n''_{q-1}} \frac{1}{i\omega^{\mathrm{F}}_{n''_2} + \ldots + i\omega^{\mathrm{F}}_{n''_{q-1}}}\frac{1}{-i\omega^{\mathrm{F}}_{n''_2}}\cdots\frac{1}{-i\omega^{\mathrm{F}}_{n''_{q-1}}}. \tag{4.22}$$

There is only one case for which the above Matsubara sum doesn't vanish, when $q = 3$. [2] In this case, the Matsubara sum has a second-order pole at the origin:

$$\Sigma_\phi(0) = J\sqrt{\frac{N}{M}}\frac{1}{\beta}\sum_{n''_2}\frac{1}{i\omega^{\mathrm{F}}_{n''_2}}\frac{1}{-i\omega^{\mathrm{F}}_{n''_2}}. \tag{4.23}$$

[2] Remark that this is the only time in this thesis that we observe a qualitative difference depending on the choice of q.

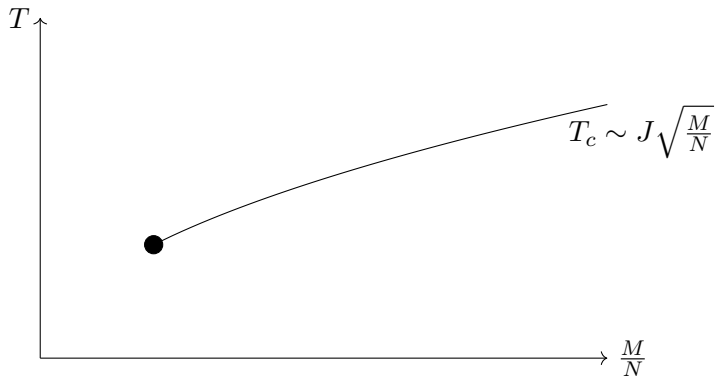

Figure 4.5: The $T - \frac{M}{N}$ plane for a given q. For large $\frac{M}{N}$ the critical temperature scales as a square root, while for small $\frac{M}{N}$ there is no critical temperature.

By using the residue theorem for second-order poles (see appendix A for details), eq. (4.23) becomes

$$\Sigma_\phi(0) = J\sqrt{\frac{N}{M}}\frac{\beta}{4}. \tag{4.24}$$

In Euclidean time, eq. (4.24) is simply

$$\Sigma_\phi(\tau) = \frac{J}{4}\sqrt{\frac{N}{M}}. \tag{4.25}$$

Since the fermionic Green's function is non-interacting in the $\frac{M}{N} \ll 1$ regime, it is $G_\psi(\tau) = (1/2)\,\mathrm{sgn}(\tau)$. From this we see that the solution eq. (4.25) is consistent with the $q = 3$ bosonic saddle point equation eq. (4.1).
Observe that eq. (4.25) is independent of temperature. So, there cannot be a phase transition of any kind in this regime of SYK*. This implies that there is no critical temperature either, meaning that the critical line we found in section 4.1 will end abruptly as shown in fig. 4.5. The appearance of such a critical point suggests that the phase transition at large $\frac{M}{N}$ is one in which no symmetries are broken, since we can "walk around" the critical line to the new phase without breaking any symmetries along the way.

4.3 Discussion and outlook

In this thesis, we introduced the SYK model and demonstrated several of its distinguishing properties. We saw how in the large-N limit the perturbative expansion was dominated by melonic diagrams which characterized the two-point function. We also saw that the four-point function were governed by ladder diagrams and learned that higher-point functions were constructed from four- and six- point functions. The infrared limit of SYK was exploited to find a conformal solution

to the Green's function before conformal symmetry was shown to indeed exist in the IR. We briefly discussed the special cases $q = 2$, which summed rainbows diagrams, and q very large, both of which yielded analytic solutions. In chapter 3 the SYK* model, which introduced an additional free parameter M (number of bosons), was presented. The model was shortly related to prior SYK models, SYK and SUSY SYK. In addition, a line was drawn between SYK* and a theory of $3+1$ dimensional SHF. We found the fermionic and bosonic self energies of SYK* by the saddle point method: integrating over the Gaussian disorder, introducing the bilocal 'Green's functions' and 'self energies' before deriving the bilocal effective action. We also reviewed the two families of conformal solutions found by Marcus and Vandoren, presenting the rational and irrational solutions. We plotted the fermionic and bosonic spectral functions: they agreed with the claim that SYK-like models do not have quasi-particle description. Finally, we proceeded to explore the parameter space of SYK*. Using the saddle point equations, the two "corners" of the $\frac{M}{N}$ parameter space were discussed, namely, $\frac{M}{N} \gg 1$ and $\frac{M}{N} \ll 1$. In the former case, a phase transition was found to occur, for which the critical temperature was given for various values of q. The latter case was found to have temperature-independent solution, implying the absence of a classical phase transition. This suggested the presence of a critical point in the $T - \frac{M}{N}$ plane. The nature of this phase transition in SYK* has yet to be fully understood, with many questions remaining unanswered: for example, what is the interpretation of the fermionic self-energy playing the role of the order-parameter governing this phase transition? What two phases is the critical boundary meant to be separating? It is conceivable that the critical point is really a tri-critical point? Because the critical point is presumably to be found somewhere in the intermediate region of large and small $\frac{M}{N}$, the presented analysis was not suited to address this further as only zeroth-order corrections were considered. One may better probe the intermediate region by considering next-to-leading order corrections in the expansion parameter $\sqrt{\frac{M}{N}}$. This can be achieved by including corrections to the Green's functions and self-energies as

$$G = G^{(0)} + G^{(1)} \quad \text{and} \quad \Sigma = \Sigma^{(0)} + \Sigma^{(1)},$$

where the superscripts (0) and (1) denote the zeroth and linear order corrections respectively. In so doing, one may be able to find these correction self-consistently by neglecting quadratic-order fluctuations. It is very likely that temperature-dependence will arise on the $\frac{M}{N} \ll 1$ side and phase-separate that regime. Such are the open questions on the SYK* model that we hope can be addressed in future research.

Appendix A

Matsubara sums

This appendix is devoted to proving the various Matsubara identities used throughout chapter 4. We begin by showing eq. (4.9), the well known relation that

$$\boxed{\frac{1}{\beta}\sum_{n\in\mathbb{Z}}\frac{-1}{i\omega_n^{\mathrm{B}}-A}=\frac{1}{e^{\beta A}-1}+\frac{1}{2}} \tag{A.1}$$

where we take $\mathrm{Re}(A)>0$ without loss of generality. By the residue theorem, we can write

$$\frac{1}{\beta}\sum_{n\in\mathbb{Z}}\frac{-1}{i\omega_n^{\mathrm{B}}-A}=\frac{1}{2\pi i}\oint_C \underbrace{\frac{-1}{z-A}\frac{1}{e^{\beta z}-1}}_{f(z)}dz, \tag{A.2}$$

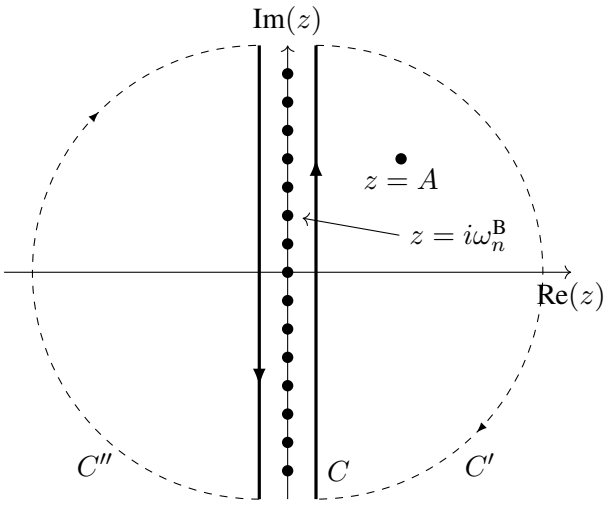

Figure A.1: Illustration of contours to perform the Matsubara sum eq. (A.1). There are poles at even Matsubara frequencies and a pole sitting at $z=A$, where we take $\mathrm{Re}(A)>0$.

where C fully encloses the imaginary axis *counter-clockwise* as shown in fig. A.1. We now consider the contribution of the infinite arcs C' and C''. For $\mathrm{Re}(z) \to \infty$, the integrand of eq. (A.2), $f(z)$, decays exponential such that the arc C' does not cost anything. For $\mathrm{Re}(z) \to -\infty$ however, the situation is different. In this limit, the integrand neither decays exponentially nor algebraically so we must consider the contribution of the line integral along C''. Parametrizing the curve by $z = Re^{i\theta}$ with $-\frac{3\pi}{2} \leq \theta \leq -\frac{\pi}{2}$, we find

$$\int_{C''} f(z)dz \overset{R\gg 1}{=} \int_{C''} \frac{1}{z}dz = i\int_{-\frac{\pi}{2}}^{\frac{\pi}{2}} d\theta = i\pi.$$

Thus, we add and subtract an $i\pi$ in eq. (A.2) such that

$$\frac{1}{2\pi i}\oint_C f(z)dz = \frac{1}{2\pi i}\left(\oint_{C+C'} f(z)dz + \oint_{C+C''} f(z)dz + i\pi\right). \tag{A.3}$$

Since the function is analytic everywhere inside the contour $C + C''$, the integral over it vanishes by Cauchy's integral theorem. The contour integral over $C + C'$ can be evaluated by the residue theorem. Accounting for the factor -1 coming from clockwise integration, eq. (A.1) follows immediately.

We now validate the more complicated looking eq. (4.16),

$$\boxed{\frac{1}{\beta}\sum_{n\in\mathbb{Z}} \frac{-1}{i\omega_n^{\mathrm{B}} - A_1}\frac{1}{i\omega_n^{\mathrm{B}} - A_2} = \left(\frac{1}{e^{\beta A_1}-1} - \frac{1}{e^{\beta A_2}-1}\right)\frac{1}{A_1 - A_2}} \tag{A.4}$$

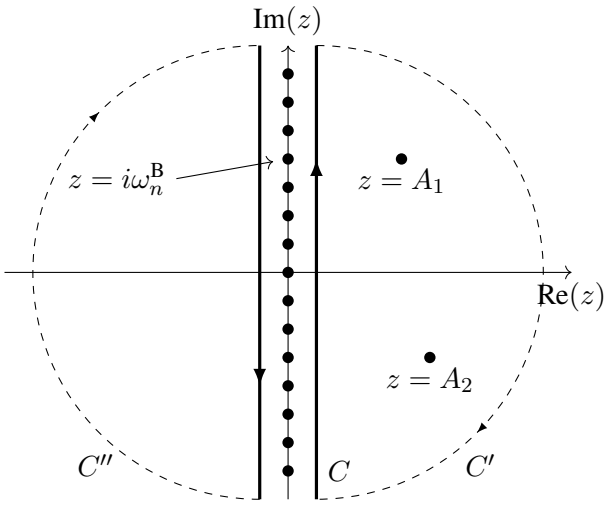

Figure A.2: Contour to evaluate Matsubara sum eq. (A.4). In addition to the pole at $z = A_1$ there is a pole at $z = A_2$. We take $\mathrm{Re}(A_1), \mathrm{Re}(A_2) > 0$.

By the residue theorem we can write

$$\frac{1}{\beta}\sum_{n\in\mathbb{Z}}\frac{-1}{i\omega_n^{\mathrm{B}}-A_1}\frac{1}{i\omega_n^{\mathrm{B}}-A_2}=\frac{1}{2\pi i}\oint_C\underbrace{\frac{-1}{z-A_1}\frac{1}{z-A_2}\frac{1}{e^{\beta z}-1}}_{f(z)}dz, \tag{A.5}$$

where C fully encloses the imaginary axis counter-clockwise (as before). Notice now that as $\mathrm{Re}(z)\to\pm\infty$, $f(z)\to 0$ (exponentially and algebraically respectively). So the arcs C' and C'' (see fig. A.2) do not cost anything to add such that we can write

$$\frac{1}{2\pi i}\oint_C f(z)dz=\frac{1}{2\pi i}\left(\oint_{C+C'}f(z)dz+\oint_{C+C''}f(z)dz\right). \tag{A.6}$$

Similar to before, the contour integral over $C+C''$ vanishes by virtue of Cauchy's theorem. This leaves the integral over $C+C'$; using the residue theorem this yields

$$\frac{1}{2\pi i}\oint_{C+C''}f(z)dz=\left(\frac{1}{e^{\beta A_1}-1}-\frac{1}{e^{\beta A_2}-1}\right)\frac{1}{A_1-A_2}, \tag{A.7}$$

where we included a -1 factor from the contour orientation. This concludes the proof of eq. (4.16).

We now verify the statements in section 4.2 that eq. (4.21) vanishes when $\omega_n^{\mathrm{B}}\neq 0$ and derive the zero-frequency $q=3$ result eq. (4.24). The first consists in showing that

$$\boxed{\frac{1}{\beta}\sum_{n\in\mathbb{Z}}\frac{1}{i\omega_n^{\mathrm{F}}-A}\frac{-1}{i\omega_n\mathrm{F}}=0}, \tag{A.8}$$

where $A=i\omega_m^{\mathrm{B}}\neq 0$. Using the residue theorem the left hand side becomes

$$\frac{1}{\beta}\sum_{n\in\mathbb{Z}}\frac{1}{i\omega_n^{\mathrm{F}}-A}\frac{-1}{i\omega_n^{\mathrm{F}}}=\frac{1}{2\pi i}\oint_C\mathrm{d}z\,\underbrace{\frac{1}{z-A}\frac{-1}{z}\frac{-1}{e^{\beta z}+1}}_{f(z)}, \tag{A.9}$$

where C encloses the entire imaginary axis *counter-clockwise* except at the location of the poles $z_1=A$ and $z_2=0$ as shown in fig. A.3. The integrand is analytic in the rest of the complex plane such that we can deform (inflate) the contours so as to only enclose the two pole z_1 and z_2 *clockwise* such that

$$\frac{1}{2\pi i}\oint_C\mathrm{d}z\frac{1}{z-A}\frac{-1}{z}\frac{-1}{e^{\beta z}+1}=\frac{1}{2\pi i}\Big[\oint_{C_1}\mathrm{d}zf(z)+\oint_{C_2}\mathrm{d}zf(z)\Big], \tag{A.10}$$

where C_1 and C_2 encloses z_1 and z_2 respectively. Using the residue theorem on these integrals yields

$$\frac{1}{2\pi i}\Big[\oint_{C_1}\mathrm{d}zf(z)+\oint_{C_2}\mathrm{d}zf(z)\Big]=\frac{1}{A}\frac{-1}{e^{\beta A}+1}-\frac{1}{A}\frac{-1}{2}. \tag{A.11}$$

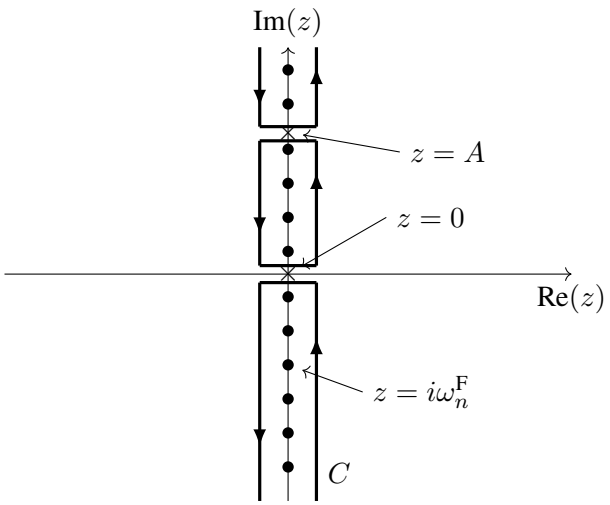

Figure A.3: Contours used to evaluate the Matsubara sum eq. (A.8). There are poles located at each fermionic (odd) Matsubara frequency and two more at $z = A$ and $z = 0$. Here A is a bosonic Matsubara frequency.

This is 0 by the fact that $e^{\beta A} = e^{\beta i\omega_n^{\mathrm{B}}} = 1$ (even Matsubara frequency).

Next we prove that at zero-frequency we have,

$$\boxed{\frac{1}{\beta}\sum_{n\in\mathbb{Z}}\frac{1}{i\omega_n^{\mathrm{F}}}\frac{-1}{i\omega_n^{\mathrm{F}}} = \frac{\beta}{4}} \tag{A.12}$$

The procedure is analogous to the previous eq. (A.8) but with $A = 0$. Rewriting the left-hand side of eq. (A.12) as

$$\frac{1}{\beta}\sum_{n\in\mathbb{Z}}\frac{1}{i\omega_n^{\mathrm{F}}}\frac{-1}{i\omega_n^{\mathrm{F}}} = \frac{1}{2\pi i}\oint_C \mathrm{d}z \underbrace{\frac{1}{z}\frac{-1}{z}\frac{-1}{e^{\beta z}+1}}_{f(z)}, \tag{A.13}$$

where C is the same as previously. The difference occurs when we deform the contour. Now there is only one degree-two pole at the origin $z = 0$. Thus we need to use the generalization of the residue theorem to higher-order poles: the residue of $f(z)$ around an order n pole is

$$\mathrm{Res}(f, z_0) = \frac{1}{(n-1)!}\lim_{z\to z_0}\frac{\mathrm{d}^{n-1}}{\mathrm{d}z^{n-1}}[(z - z_0)^n f(z)]. \tag{A.14}$$

Then, by straightforward application of eq. (A.14) for $n = 2$, we find

$$\frac{1}{2\pi i}\oint_{C'} \mathrm{d}z f(z) = \frac{\beta}{4}, \tag{A.15}$$

where C' encloses the origin *clockwise*. Equation (A.12) is thus proved.

Bibliography

[1] S. Sachdev and J. Ye. Gapless spin-fluid ground state in a random quantum heisenberg magnet. *Physical Review Letters*, 70(21):3339, 1993.

[2] A. J. Bray and M. A. Moore. Metastable states in spin glasses. *Journal of Physics C: Solid State Physics*, 13(19):L469, 1980.

[3] S. Sachdev. Holographic metals and the fractionalized Fermi liquid. *Physical Review Letters*, 105(15):151602, 2010.

[4] J. Polchinski and V. Rosenhaus. The spectrum in the Sachdev-Ye-Kitaev model. *Journal of High Energy Physics*, 2016(4):1, 2016.

[5] A. Kitaev. A simple model of quantum holography. Entanglement in Strongly-Correlated Quantum Matter, 2015.

[6] A. Kitaev. A simple model of quantum holography. Entanglement in Strongly-Correlated Quantum Matter, 2015.

[7] P. Kuusela. SYK and SYK-like models. Master's thesis, University of Helsinki, 2017.

[8] G. 't Hooft. A planar diagram theory for strong interactions. In *The Large N Expansion In Quantum Field Theory And Statistical Physics: From Spin Systems to 2-Dimensional Gravity*, pages 80–92. World Scientific, 1993.

[9] W. Fu. *The Sashdev-Ye-Kitav model and matter without quasiparticles*. PhD thesis, Harvard University, 2018.

[10] Z. Bi, C. M. Jian, Y. Z. You, K. A. Pawlak, and C. Xu. Instability of the non-fermi-liquid state of the Sachdev-Ye-Kitaev model. *Physical Review B*, 95(20):205105, 2017.

[11] C. M. Varma, Z. Nussinov, and W. Van Saarloos. Singular or non-Fermi liquids. *Physics Reports*, 361(5-6):267–417, 2002.

[12] Y. Wang. A solvable random model with quantum-critical points for non-Fermi-liquid pairing. *arXiv:1904.07240*, 2019.

[13] J. Maldacena. The large-N limit of superconformal field theories and supergravity. *International Journal of Theoretical Physics*, 38(4):1113–1133, 1999.

[14] M. Ammon and J. Erdmenger. *Gauge/Gravity Duality: Foundations and Applications*. Cambridge University Press, 2015.

[15] E. Witten. An SYK-like model without disorder. *arXiv:1610.09758*, 2016.

[16] R. Gurau. Invitation to random tensors. *arXiv:1609.06439*, 2016.

[17] V. Rosenhaus. An introduction to the SYK model. *arXiv:1807.03334*, 2018.

[18] D. Gross and V. Rosenhaus. A generalization of Sachdev-Ye-Kitaev. *Journal of High Energy Physics*, 2017(2):93, 2017.

[19] W. Fu, D. Gaiotto, J. Maldacena, and S. Sachdev. Supersymmetric SYK models. *arXiv:1610.08917*, 2016.

[20] J. Murugan, D. Stanford, and E. Witten. More on supersymmetric and 2d analogs of the SYK model. *Journal of High Energy Physics*, 2017(8):146, 2017.

[21] G. J. Turiaci and H. Verlinde. Towards a 2d QFT analog of the SYK model. *Journal of High Energy Physics*, 2017(10):167, 2017.

[22] P. Zhang. Dispersive Sachdev-Ye-Kitaev model: band structure and quantum chaos. *Physical Review B*, 96(20):205138, 2017.

[23] Y. Gu, X. L. Qi, and D. Stanford. Local criticality, diffusion and chaos in generalized Sachdev-Ye-Kitaev models. *Journal of High Energy Physics*, 2017(5):125, 2017.

[24] S. Banerjee and E. Altman. Solvable model for a dynamical quantum phase transition from fast to slow scrambling. *Physical Review B*, 95(13):134302, 2017.

[25] E. Marcus and S. Vandoren. A new class of SYK-like models with maximal chaos. *Journal of High Energy Physics*, 2019(1):166, 2019.

[26] T. G. Mertens. The Schwarzian theory—origins. *Journal of High Energy Physics*, 2018(5):36, 2018.

[27] E. Marcus. Holography and the Sashdev-Ye-Kitaev model. Master's thesis, Utrecht University, 2017.

[28] L. Cugliandolo. Disordered systems. Laboratoire de Physique Théorique et Hautes Energies de Jussieu, May 2011.

[29] V. Bonzom, V. Nador, and A. Tanasa. Diagrammatic proof of the large-N melonic dominance in the SYK model. *arXiv:1808.10314*, 2018.

[30] J. Maldacena and D. Stanford. Remarks on the Sachdev-Ye-Kitaev model. *Physical Review D*, 94(10):106002, 2016.

[31] D. Gross and V. Rosenhaus. All point correlation functions in SYK. *Journal of High Energy Physics*, 2017(12):148, 2017.

[32] V. P. J. Jacobs, S. Grubinskas, and H. T. C. Stoof. Towards a field-theory interpretation of bottom-up holography. *Journal of High Energy Physics*, 2015(4):33, 2015.